Available online at www.sciencedirect.com
SCIENCE DIRECT®
Journal of Solid State Chemistry 178 (2005) 2491–2510
JOURNAL OF SOLID STATE CHEMISTRY
www.elsevier.com/locate/jssc

Flexibility in metal-organic framework materials: Impact on sorption properties

Ashleigh J. Fletcher[a], K. Mark Thomas[a,*], Matthew J. Rosseinsky[b]

[a]*Northern Carbon Research Laboratories, Department of Chemistry, Bedson Building, University of Newcastle-upon-Tyne, Newcastle-upon-Tyne, NE1 7RU, UK*
[b]*Department of Chemistry, University of Liverpool, Liverpool L69 7ZD, UK*

Received 16 March 2005; accepted 13 May 2005

Abstract

Recent years have seen the development of a new class of porous coordination polymers known collectively as metal organic framework materials (MOFs). This review outlines recent progress in understanding how adsorption characteristics of these systems differ from rigid classical sorbents such as activated carbon and zeolites. Gas/vapor adsorption studies for characterization of the porous structures of MOF materials are reviewed and differences in adsorption characteristics based on detailed measurement of equilibrium and dynamical sorption behavior, compared with previous generations of sorbents, are highlighted. The role of framework flexibility and specific structural features, such as windows and pore cavities, within the MOF porous structures are discussed in relation to adsorption mechanisms.

Keywords: Metal organic framework materials; Sorption; Porous materials; Pore windows; Framework flexibility; Adsorption dynamics

1. Introduction

Recent years have seen the evolution of a new class of coordination polymers known collectively as metal organic framework materials (MOFs) [1–4]. These materials are formed by coordinate bonds from multidentate ligands to mono- or polynuclear metal centers and may have extensive open-framework structures resulting in the inclusion of guest species (usually solvent) during synthesis. These species can be removed via desolvation and the resulting empty framework may maintain structural integrity giving a porous MOF material, which has a large apparent surface area. The original solvent or other guest molecules can then be adsorbed into this porous structure. The MOF connectivities and topologies are controlled by the coordination preferences of metal and ligand, with the templating role of pore species being less pronounced in structure direction than it is in zeolitic aluminosilicate and metallophosphate systems governed by template-directed assembly of purely tetrahedral building units.

Porous media have potential applications in many fields including separation, heterogeneous catalysis, and gas storage. Porous networks are also of interest because

Abbreviations: azpy, trans-4, 4′-azopyridine; bdc, benzenedicarboxylate; bpdc, 4, 4′-biphenyldicarboxylate; bipy, bipyridine; bpp, 1, 3-bis(4-pyridyl)propane; bpydc, 2, 2′-bipyridyl-5, 5′-dicarboxylate; BTB, 4, 4, 4″-benzen-1, 3, 5-triyl-tribenzoate; btc, benzene-1, 3, 5-tricarboxylic acid; cyclam, 1, 4, 8, 11-tetrazocyclotetradecane; DAB, diaminobutane; DABCO, 1, 4-diazabicyclo[2.2.2]octane; DBM, dibenzoylmethanate; dhbc, dihydroxybenzoic acid; DMF, dimethylformamide; dpyg, 1, 2-di(4-pyridyl)glycol; edtpn, ethylendiaminetetrapropionitrile; hpdc, pyrazoledicarboxylic; in, isonicotinate; ndc, 2, 6-naphthalenedicarboxylate; Nttpy, 4′-(*p*-nicotinamide-*N*-methylphenyl)-2, 2′:6′, 2″-terpyridine; pd, 1, 2-propandiol; pda, 1, 4-phenylendiacetate; 4-peia, *N*-(2-pyridin-4-yl-ethyl)-isonicotinamide; pia, *N*-pyridylisonicotinamide; 3-pic, 3-picoline; pyz, pyrazine; pzdc, pyrazine-2, 3-dicarboxylate; tmbdc, 2, 3, 5, 6-tetramethylbenzene-1, 4-dicarboxylate; tpt, 2, 4, 6-tri(4-pyridyl)-1, 3, 5-triazine

*Corresponding author. Fax: +44 191 222 6929.
E-mail address: mark.thomas@ncl.ac.uk (K.M. Thomas).

0022-4596/$ - see front matter © 2005 Elsevier Inc. All rights reserved.
doi:10.1016/j.jssc.2005.05.019

of adsorption properties, where confined species may alter the physical properties of the host material. MOF materials have nanometer-sized channels with tailorable chemical functionality and are thus in principle attractive for the manipulation and transformation of a wide range of molecules.

Applications of MOFs that have been demonstrated, in proof of principle, include chemical sensing [5–8], chemical catalysis [9], light to electrical energy conversion [10] and size selective membrane transport [11]. An isoreticulated MOF, which is a variant of IRMOF-1, has been reported that shows selective adsorption between para- and ortho-xylene (by a factor of 2.5 times) [12]. Research into the use of MOFs for separation processes found that $Cu_3(1,3,5\text{-btc})_2(H_2O)_3$, which has pores of 7–8 Å diameter, showed selectivity for ethylene over ethane, carbon dioxide over methane, for use in syn-gas applications, and carbon dioxide and nitrous oxide over nitrogen and oxygen, for purification of air [13]. This material also displays heterogeneous catalytic activity for cyanosilylation of benzaldehyde [14]. Further applications will emerge as new materials are developed.

Gas adsorption studies, in particular nitrogen adsorption at 77 K, are routinely used for the characterization of porous structures. In the case of MOFs with pore dimensions of $<\sim$0.5 nm, activated diffusion [15,16] may occur at 77 K preventing the observation of nitrogen uptake. In these circumstances, adsorption of carbon dioxide at 273 K may be used as a routine measurement for estimation of micropore volume. These routine measurements will not be discussed in detail unless they show unusual characteristics, which demonstrate the unique features of MOF systems. In order to understand the capabilities and limitations of MOF systems in this regard, fundamental information on their response to guests is invaluable.

2. Development of metal organic framework porous structures

Kitagawa proposed [2] that it is impossible to synthesize compounds containing vacant spaces, as nature abhors a vacuum. Hence, the pores will always initially be filled with some sort of guest or templating molecules. The guest species are important both through their role in determining the nature of the porous structure which assembles around them and because they need to be sufficiently volatile or exchangeable to permit either the generation of a truly porous material or other molecules to occupy the pore structure. The MOF systems allow access to open-framework structures with network topologies and connectivities that are not usually observed in classical porous materials, and one attraction is the possibility of generating unusually large diameter channels and cavities. However, using large linkers to create micropores is not always successful as it may lead to network interpenetration, thus actually reducing the effective pore volume created. An alternative strategy is to design a framework, in which the spaces occur topologically, e.g. the diamond and graphene nets or the B net in CaB_6 [17–20]—are frequently used in construction of highly porous coordination polymers. This designed "node and spacer" approach has been extensively documented by Yaghi, O'Keeffe and co-workers, and demonstrated to be a powerful approach for the synthesis of a variety of topologies, permitting the development of families of materials with the same connectivity but tunable pore dimensions. It has recently been conceptually extended to the actual assembly of pre-synthesized molecular building units into identifiable frameworks by Férey and co-workers in the MIL-10n series of materials [21,22].

The permanent porosity present in classical rigid adsorbents is considered to be associated with the structural rigidity of the constituent bonds, e.g. Si–O in zeolites or C–C bonds in carbon adsorbents. The higher thermal and chemical stability of classical adsorbents, in comparison with the new generation of coordination framework materials means that these new porous structures must provide new mechanisms for adsorption/desorption or transformation behavior to compete for use in associated applications. This is possible due to the extra internal degrees of freedom (rotation, torsion, vibration) evident in MOFs, which allows flexibility to be conferred on the materials [23,24].

2.1. Porous structure and dimensionality

This article focuses on specific examples of MOF materials with unusual sorption function related to flexibility. Due to the diversity of organic linkers and mono- and polynuclear inorganic components, a wide-ranging survey of structure types is beyond the scope of the current paper. A comprehensive analysis of structure classified by pore dimensionality has been given recently by Kitagawa et al. [2] and is summarized below.

2.1.1. Isolated cavities ("zero dimensions")

Such systems are generated when windows are not present or are small compared with guest molecule dimensions preventing communication between them via transport of guest molecules. This is quite a rare situation but is realized in $[Zn(CN)(NO_3)(tpt)_{2/3}\cdot\frac{3}{4}C_2H_2Cl_4\cdot\frac{3}{4}CH_3OH]_n$ [25] where the cavity is formed by six octahedrally arranged $Zn_4(CN)_4$ squares with cations at the corners and edges bridged by cyanide—these squares are linked by three connecting 2,4,6-tri(4-pyridyl)-1,3,5-triazine (tpt) molecules and the cages are linked by sharing squares. Interpenetration of two of these nets produces a structure with large (containing 20 solvent molecules) cavities that are completely isolated

from each other. Such systems are of course non-porous. It is more usual for adjacent cavities to be accessible, giving rise to the pore connectivities outlined below.

2.1.2. One-dimensional channels

This is a common motif [2,26–33]. An interesting recent example [34] (Fig. 1) involves triangular channels formed by an overlapping triangular array of linear coordination polymer chains formed by aromatic dicarboxylates binding to macrocyclic $Ni(cyclam)^{2+}$ complexes linked weakly by C–H…π interactions between the macrocycle and the aromatic π system—the ability of such a weak interaction to stabilize permanent porosity is a recurring feature in MOF materials and is often important in conferring flexibility on their porosity.

2.1.3. Two-dimensional space

There are many examples of structures that incorporate layers with guests occupying the two-dimensional (2D) space between layers which provide a barrier in the third dimension due to dense packing without voids [2]. However, permanent porosity in such materials is rare, presumably due to turbostratic disorder induced by layer sliding upon guest loss. These systems do however have a very rich guest exchange chemistry [35].

2.1.4. Three-dimensional porosity

Zeolites such as sodalite and faujasite contain channels that intersect in three dimensions. This is more difficult to engineer in MOF systems although highly symmetrical cubic systems based on designed secondary building units such as the IRMOF [1] and MIL [21] series as well as the chiral (10,3)-*a* network phases of framework composition M_3btc_2 [36] do display three-dimensional (3D) permanent porosity. The latter feature non-linear helical porosity, which also follows the (10,3)-*a* structure (Fig. 2(c)). There are a large number of systems where layers are pillared into three dimensions by a second group producing pseudo-three-dimensional porosity in which one of the channel dimensions is considerably greater than the other two (Figs. 3 and 4).

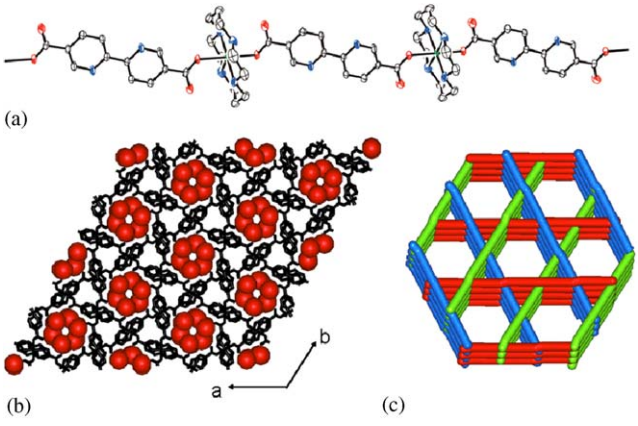

Fig. 1. A 1D pore system. X-ray structure of [Ni(cyclam)(bpydc)]·$5H_2O$ (a) Structure of the linear coordination polymer. (b) View on the *ab* plane showing the linear coordination polymer chains extending in three directions; water guest molecules occupying the channels are depicted in CPK style (red). (c) View showing the stacking of the linear chains, which generates 1D channels [34].

It is useful to consider how these structures can be formed by breaking down the roles played by metal centers, framework-forming multidentate ligands and auxiliary non-framework forming ligands bound to the metal center.

Mononuclear metal, charged framework-forming ligand, neutral framework: 3D permanent porosity is rarely achieved by a single metal center coordinated to a single framework-forming ligand without any coordination of auxiliary ligands at the metal center. The Ni_3btc_2(3-picoline)$_6$(1,2-propandiol)$_3$ system is permanently porous with chiral 3D porosity but the auxiliary alcohol and aromatic amine ligands at the metal center are instrumental in stabilizing the guest-free structure via C–H…π hydrogen bonding [36].

Mononuclear metal, neutral framework-forming ligand: Charged mononuclear metal porous frameworks result when the framework-forming ligand is neutral, thereby requiring an auxiliary anion to generate neutrality—in the case of bipyridyl-based systems porosity is favored when the ligand binds to the metal, as nitrate does, rather than occupying the channels. An example of this is the two Ni_2(4,4′-bipy)$_3(NO_3)_4$ polymorphs both based on T-shaped coordination of three bipyridyl ligands to the metal which are porous due to this motif (Fig. 2) [37]. The porosity of these materials is notable for its complex structure in which relatively large cavities are interconnected via narrower windows, a feature we will return to in discussing the detailed sorption properties of these materials.

The distinction between charged and neutral frameworks is not a trivial one—the charged defects in aluminosilicate zeolite frameworks are associated with their catalytic activity, while neutral zeotype frameworks are generally more demanding to instill catalytic activity in.

Mononuclear metal, multiple framework-forming ligands: The charge-compensating anion in the examples above can also play the role of framework-former in connecting 1D or 2D metal-organic moieties into 3D networks. Cu(4,4′-bipy)SiF_6 features a 2D square motif formed by coordination of four linear bipyridyl linkers to a metal center—large 1D channels passing through the square grid centers are produced by connection of these layers by the bidentate inorganic SiF_6^{2-} unit binding to copper sites in adjacent layers [19]. The porosity is actually three-dimensional as considerably smaller channels exist parallel to the layer, limited by the inorganic anion.

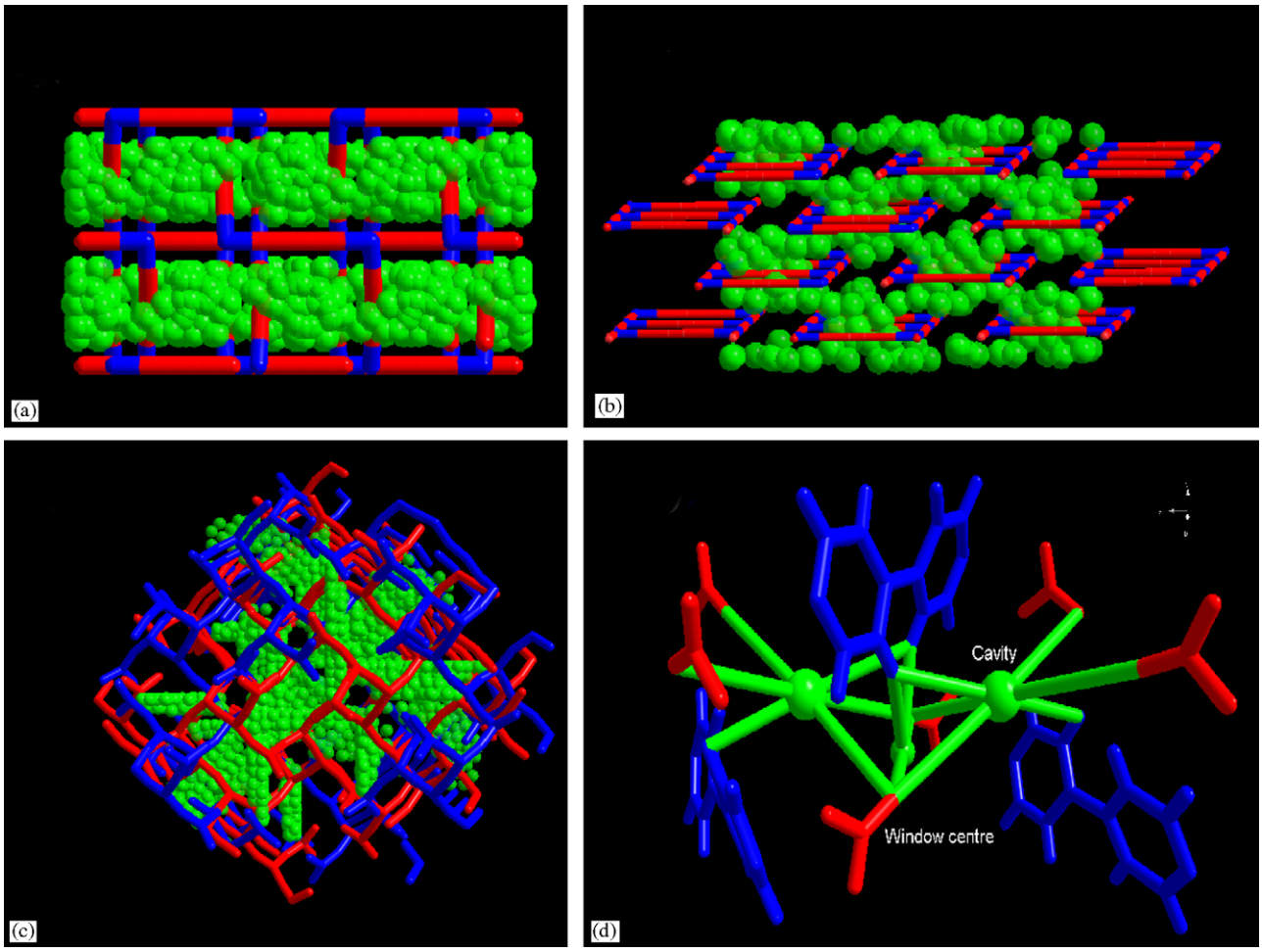

Fig. 2. Crystal structures of porous MOF materials with charged (**M**, **E**) and neutral (**C**) frameworks. The frameworks are represented by blue and red solid lines connecting metal and bridging ligand centers. The extra-framework void volume is represented as green spheres of radius 1.2 Å (a) and (b) are polymorphs of the same composition $Ni_2(4,4'\text{-bipy})_3(NO)_4$. (a) **E** This material has windows of dimension 2.32×2.75 Å giving access to cavities $5.4 \times 5.2 \times 4.1$ Å (the cavities in the loaded material contain ethanol guests of dimensions $4.2 \times 4.3 \times 6.3$ Å) and a pore volume of $0.149\,cm^3\,g^{-1}$. (b) **M** windows 2.5×4.9 Å, cavities $4.3 \times 5.3 \times 8.3$ Å and a pore volume of $0.181\,cm^3\,g^{-1}$. (c) **C** has composition $Ni_3btc_2(3\text{-picoline})_6(1,2\text{-propandiol})_3$ and is chiral, adopting the (10,3)—a network structure. It has windows 8.5×8.5 Å, cavities 13.7×10.7 Å and a pore volume of $0.63\,cm^3\,g^{-1}$. (d) The closest framework contacts to the cavity center (large green sphere) and window aperture (small green sphere) in phase **E**. Bipyridyl groups from the framework structure are represented in blue, and metal-bound nitrate anions are highlighted in red. The channels run parallel to the crystallographic *a*-axis; the large cavities and much smaller windows alternate along this direction such that each cavity is separated by a small aperture. The contact distances for the pore cavities are 5.4 and 4.25 Å to *trans*-nitrate anions and bipyridyl ligands, respectively; the shortest contact to the framework at the window aperture is 2.52 Å, giving the window dimension as 2.2 Å. All distances quoted take into account the van der Waals radii [37].

Polynuclear metal centers—secondary building units and "superclusters": The "jungle gym" structures of M_2(1,4-benzenedicarboxylate)$_2$(1,4-diazabicyclo[2.2.2]octane) involve neutral square inorganic layers linked by the neutral organic linker DABCO to give a 3D framework, but now feature a dinuclear metal cluster bridged by carboxylate groups as the building unit (Figs. 3 and 4) [38]. These metal cluster units form the basis of a "secondary building unit" approach to neutral framework structures exemplified by the cubic Cu_3(1,3,5-btc)$_2(H_2O)_3$ material [39]. The $Zn_4O(O_2CRCO_2)_6$ cluster acts as an octahedral node in generating the cubic net of the highly stable MOF-5 [17] which is the parent of a family of isoreticular frameworks [1] with the same structure but varying pore dimensions. Such metal clusters can themselves be arranged in "supercluster" units as in the case of MIL-100 where triconnecting btc anions link four Cr_3O units into a supertetrahedron, which themselves share corners to generate a material with cages up to 29 Å in diameter (Fig. 5). In this case the $Cr_3O(O_2CRCO_2)_6$ units give the framework a positive charge, which is balanced by fluoride anions [22].

2.2. Characterization of porosity in MOFs

A porous material must retain its structural integrity during adsorption and desorption of guest species. It is

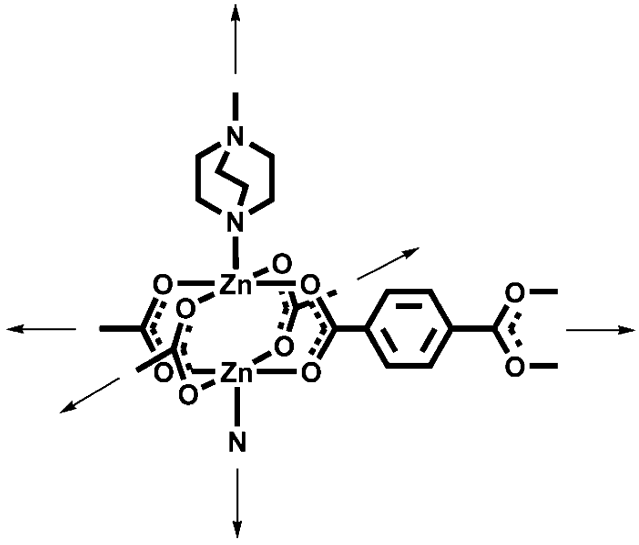

Fig. 3. 3D porosity produced by linking a 2D layer. The extension of the 2D square-grid of $[Zn_2(1,4\text{-bdc})_2]$, formed by bridging of zinc carboxylate dimer species, into a 3D structure by using DABCO, which occupies the axial positions [38].

possible to use thermo-gravimetry to determine the temperature at which guest species are lost and the temperature at which the evacuated structure becomes unstable and ultimately decomposes. It must be stressed that for many materials the temperature at which both of these processes occur is the same and a stable evacuated material may never be obtained. The presence of permanent porosity can be characterized by gas adsorption/desorption isotherms [17,39–55], (outlined in Section 3). Surface area is the parameter widely used for the characterization of porous structures but it is not an unequivocal quantity since it depends on experimental parameters such as temperature, adsorbate, etc. Porous structure characteristics such as total pore and micropore volumes are also useful parameters. MOFs have been produced with a wide variety in surface area, ranging from 500 to 4500 $m^2 g^{-1}$ [19,28,39,46,51,56–58], which is much greater than the theoretical maximum value obtained for carbon adsorbents ($\sim$2630 $m^2 g^{-1}$ based on the coverage of the two sides of a graphene sheet). This is due to pore filling effects and does not necessarily represent a true surface area.

The production of a stable evacuated material has been supported by X-ray powder diffraction (XRPD) measurements, which demonstrate the close structural relationship between the solvated and desolvated materials. These results have been strengthened by recent studies involving single crystal X-ray diffraction [26,59], allowing the detection of evacuated channels and suggesting that the relative thermal instability of MOFs, often $<$473 K, stems from the relatively weaker coordination bonds present in the structure.

3. Flexibility and structural changes

Adsorption of guest molecules onto solid surfaces (i.e. an adsorbent) is essential in determining the properties of porous compounds, and is a function of both the guest molecule–surface interactions, and pore size and topology. Pores present in such materials are classified according to the IUPAC scheme [60], and may be made of exclusively one pore size or a distribution of pore widths. Macropores ($d = 50 +$ nm) are similar in adsorption behavior to open surfaces, adsorption in mesopores ($d = 2-50$ nm) is characterized by capillary condensation, resulting in an associated hysteretic loop typically in the mid-relative-pressure region. Micropores (<2 nm) exhibit enhanced adsorption due to the increased energetics of the void space associated with overlapping of the potential field of the pore walls.

There are six recognized isotherm types, as classified by Brunauer, Deming, Deming and Teller (BDDT system) as shown as in Fig. 6 [61]. The shape obtained provides information about the characteristics of the adsorbent used. Microporous materials generally produce Type-I isotherms [61,62], where the mass increases steeply at low relative pressure before reaching a plateau once the available porous structure is occupied [63–72]. Types-II, -III and -VI isotherms are mainly indicative of non- or meso/macroporous materials, while types IV and V suggest the presence of mesoporosity. Types-II and -IV isotherms are obtained for similar systems, which exhibit differences in the strength of adsorbate–adsorbent and adsorbate–adsorbate interactions. A similar relationship exists for Types -III and -V isotherms.

There has been a significant amount of literature published concerning adsorption systems and their relative characteristics, including adsorption on zeolites, activated carbons and MOFs [63–73]. In contrast to the spherical or slit-shaped pores, usually observed in zeolites or active carbons, MOFs incorporate pores with crystallographically well-defined shapes including square [19,74], rectangular [74–78] and triangular [74], sometimes connected by windows [37,54,79,80], which may exhibit different adsorption properties (Fig. 7) [74]. The pores in MOFs have a very uniform distribution unlike in heterogeneous carbon materials where a broad pore size distribution may be observed.

Gurvitsch's rule states that the adsorption uptake at relative pressure, $p/p^0 \sim 1$, when expressed as a volume of liquid (using the normal liquid density) should be the same for all adsorptives on a given adsorbent [81]. The rule is generally valid; within a few percent and minor discrepancies usually arise from small differences in the adsorption interactions. The general conformity of Gurvitsch's rule suggests that the adsorbate condenses within the porous structure having a density close to the bulk liquid density of the adsorbate [62]. Deviations are

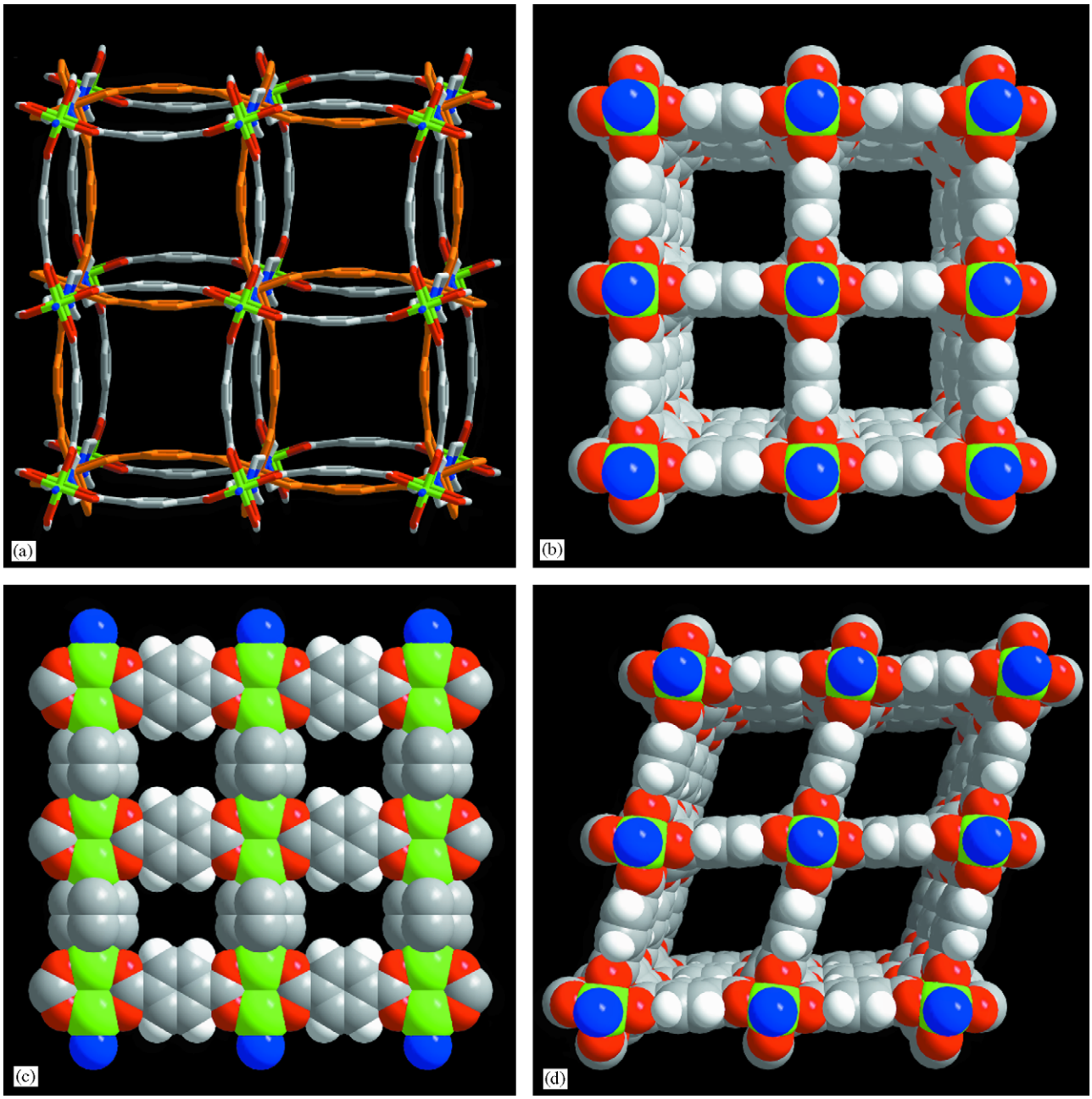

Fig. 4. (a) The view along fourfold axis of the metal-organic framework structure in $[Zn_2(1,4\text{-bdc})_2](DABCO)\cdot 4DMF\cdot \frac{1}{2}H_2O$. One $[Zn_2(1,4\text{-bdc})_2]$ 2D layer is colored orange to emphasize the alternation of stacking layer. Hydrogen atoms and guest molecules are omitted. The resulting porosity is three-dimensional; (b) space-filling representation of evacuated framework 1, which emphasizes the open square channels; view along fourfold axis. (c) Side view of evacuated framework 1, showing the windows interconnecting the channels. (d) Space-filling representation of the metal-organic framework structure in $[Zn_2(1,4\text{-bdc})_2](DABCO)\cdot 2C_6H_6$, showing rhombic-grid motif of $[Zn_2(1,4\text{-bdc})_2]$ layers. The guest molecules and DABCO hydrogens are not shown. Legend: Zn green; N blue; O red; C gray; H white [38].

often due to size effects, such as molecular sieving, where larger molecules are excluded from part of the porous structure [82]. Interestingly, it has been observed that the **M** polymorph of $Ni_2(4,4'\text{-bipy})_3(NO)_4$ does not obey the rule for ethanol adsorption, even though it has uniform porosity [80]. In this case, it is the available cavity volume that limits the adsorption capacity, which is saturated below the level predicted from adsorption of the template.

Structural flexibility has been observed in inorganic frameworks [83–88], for example, the structure of ASU-16, $Ge_{14}O_{29}F_4[H_2DAB]_3[DAB]_{0.5}\cdot 16H_2O$, shows flexibility by contracting significantly (~6%), without any loss of structural integrity, on solvent loss [83].

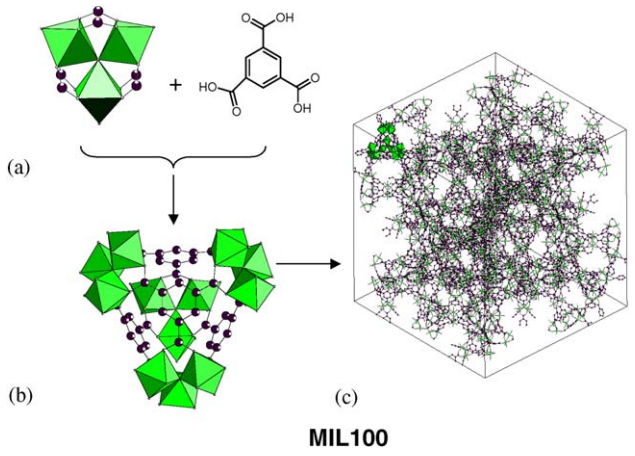

Fig. 5. (a) MIL-100 is formed by designed assembly of isolable SBUs with independent existence in solution. The original building block with a trimer of metal octahedra chelated by three carboxylic functions. (b) The supertetrahedra (ST) formed by using trimesic acid, which occupies the faces of ST. (c) Ball-and-stick view of a unit cell of MIL-100; one supertetrahedron is represented by using octahedra for a better understanding. Free water molecules have been omitted for clarity [22].

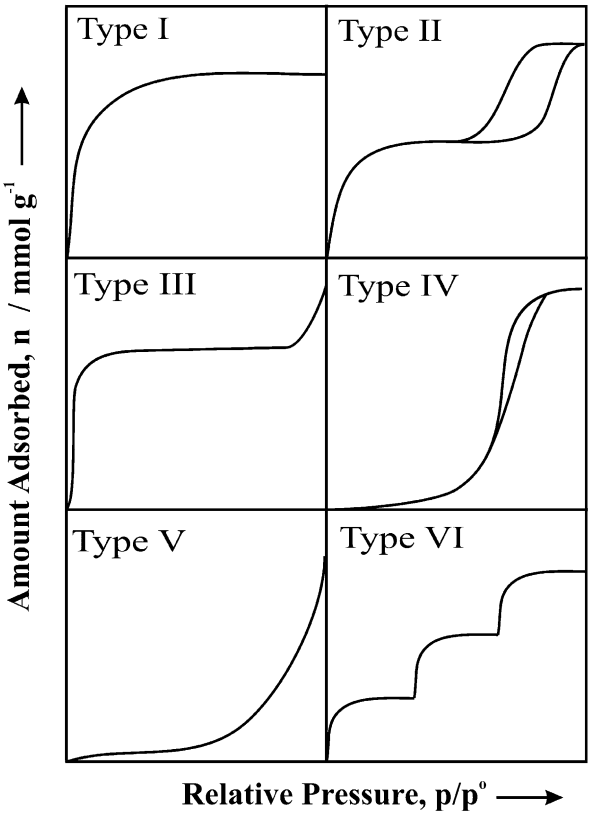

Fig. 6. Diagrammatic representation of isotherm classification: *Type I*—typical of predominantly microporous adsorbents with majority of uptake below $p/p^0 = 0.1$. *Type II*—typifies physical adsorption of gases by non-porous or mixed meso/macroporous solids, with multilayering at high relative pressures. *Type III*—characteristic of weak adsorbate–adsorbent interactions and most commonly associated with both non- and microporous adsorbents. *Type IV*—hysteretic adsorption, commonly associated with mesoporosity, where capillary condensation gives rise to a hysteresis loop. *Type V*—characteristic of weak adsorbate–adsorbent interactions and indicative of microporous or mesoporous solids. *Type VI*—introduced primarily as a hypothetical isotherm, the shape is due to the complete formation of monomolecular layers before progression to a subsequent layer.

However, the changes are not as severe as those of MOFs due to weaker interactions, including coordination bonds, H-bonds, π-electron stacking and van der Waals interactions.

Structural transformations by guest molecule inclusion are not common in zeolites but several examples of reversible structural transformations have been observed for MOFs. These include systems using both hydrophilic and hydrophobic adsorbates (guest molecules), including water, alcohols, ketones, ethers, aromatic and aliphatic molecules, where exposure is via either the liquid or vapor phase [8,35,41,49,50,53,54,89–113]. It is noteworthy that supercritical gases (nitrogen, oxygen, methane) may also cause structural transformation [114,115]. Structural transformations can include stretching, rotational, 'breathing' and scissoring mechanisms, which all induce different effects in the structure.

Stretching motions around the connector and/or linker, resulting from bond formation/cleavage, cause a structural change and usually involve weak interactions, such as hydrogen bonds, semi-coordination [116], or Jahn–Teller distortions. Hysteresis has been observed for $\{[Cu_2(pzdc)_2(dpyg)] \cdot 8H_2O\}_n$, where the 3D pillared-layer structure undergoes a structural transformation during the adsorption process, attributed to cleavage/formation of the Cu^{II}–carboxylate bond. X-ray studies show that the channels in the material contract and expand, varying between 9.6 and 13.2 Å during adsorption with a 27.9% reduction in cell volume on contraction. The structure adsorbs methanol and water but not methane at 298 K (Fig. 8), due to structural transformation for two former adsorbates [94]. However, the framework does not adsorb nitrogen [2] and these differences may be partly due to activated diffusion effects [15,16].

The structural flexibility of the **E** polymorph (Fig. 2(a)) of $[Ni_2(4,4'\text{-bipy})_3(NO_3)_4]$ demonstrates a scissoring motion for adsorption of the template ethanol and methanol, which induces a cell volume change of several percent. Both these guests are too large to pass through the windows, if the structure was rigid, and flexibility is required to allow this to take place. The relative dimensions of the cavities, occupied by the ethanol template molecules in the as-grown material, and the windows interconnecting them indicate that this type of relaxation will be required to permit the free passage of guest molecules during adsorption and desorption processes. The structure also undergoes

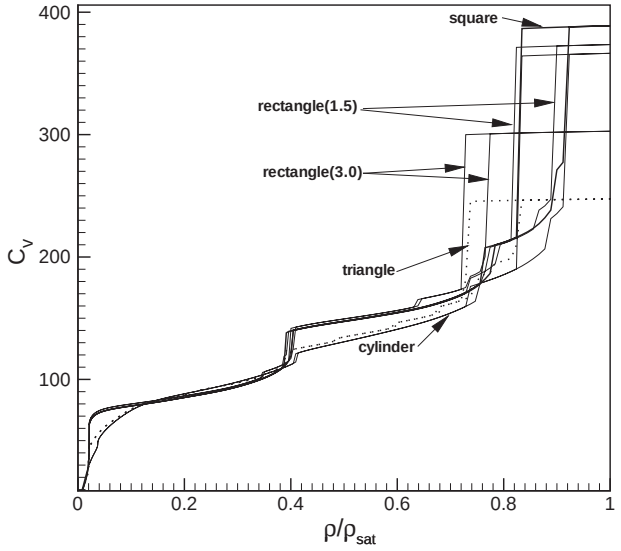

Fig. 7. Adsorption in the center slice $Cv\left[Cv \equiv (\sigma/z_1)\int_{z'}^{z'+1} aP(\vec{s},z)\,\mathrm{d}\vec{s}\,\mathrm{d}z\right]$ versus saturation p/p^0 for a 20σ square pore (thick line), a 23σ diameter cylindrical pore (thin line), a rectangular pore with a 1.5 aspect ratio and a 16σ short side (thin line), a rectangular pore with a 3.0 aspect ratio and a 10σ short side (thin line), and a right triangular pore with a 22σ short side (thick dotted line) [74].

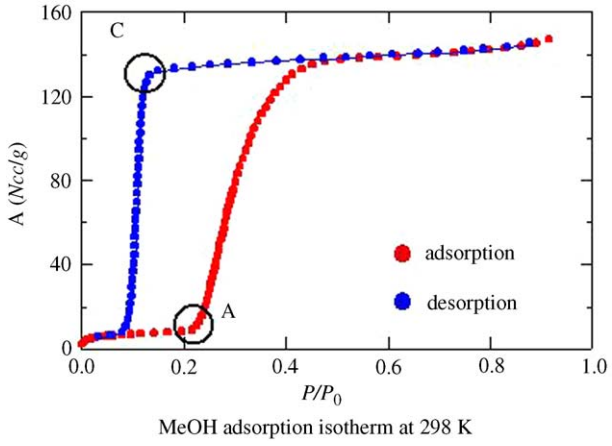

Fig. 8. Methanol adsorption (filled circles) and desorption (open circles) isotherms on $\{[Cu_2(pzdc)_2(dpyg)]\cdot 8H_2O\}_n$ at 298 K. A = absolute absorption. The isotherm shows a sudden rise at point A (relative pressure, p/p^0, is 0.23) and attains a saturated level (ca. 6.2 mmol g^{-1}) at point B ($p/p^0 = 0.5$). On the other hand, the desorption isotherm does not trace the adsorption one any more, instead, showing an abrupt drop at point C ($p/p^0 = 0.1$) [94].

structural changes during adsorption of methanol to allow adsorption on different surface sites after the complete occupation of the nitrate sites [54,97]. The methanol-derived polymorph of the same composition, which features one-dimensional coordination polymer ladders linked by C–H…O hydrogen bonds between the bipyridyl framework-forming ligands and the auxiliary anion bound to the metal, admits toluene molecules into the cavities despite this guest having twice the cross-sectional area of the windows it needs to pass through to access its eventual location [97]. Adsorption studies on MOFs have shown that the structures contain windows and pore cavities, which control diffusion into the porous structure.

Time-resolved, in situ single-crystal X-ray diffraction studies have been used to study flexibility during sorption on Co(4,4′-bipy)$_{1.5}$(NO$_3$)$_2\cdot$(guest). The framework undergoes a "*garden-trellis*"*-like* action of the bilayers, which allows accommodation of guests of varying size/shape. Adsorption of dicholoromethane induces a framework–framework transition with an associated change in symmetry. Guest sorption influences some disordered components and the torsion angles of the bipy ligands, however, no underlying trend was observed. These observations support previously published results, obtained by X-ray powder diffraction, on the distortion of the Ni-bipy analogues (**M** and **E**) during sorption of methanol and ethanol [54,80,97]. This provides new evidence that host–guest interactions may drive framework flexibility [117].

Modeling the adsorption kinetics of methanol on the **M** and **E** polymorphs of Ni$_2$(4,4′-bipyridine)$_3$(NO$_3$)$_4$ has allowed the subsequent resolution of two barriers in the adsorption processes related to diffusion through (a) windows and (b) pore cavities. Diffusion through the windows has a higher activation energy associated with it than diffusion along the pores [80]. Similar rationale has recently been used to determine the rate constants for two concurrent processes involved in the adsorption of water on evacuated ionic crystals of macrocation-Dawson-type polyoxometallates, where the authors have ascribed the two components to (a) molecular diffusion of water within the voids and (b) the large increase in *c*-axis length on water sorption [118].

Rotation around a single bond provides structure flexibility [55,93,104,119], for example, within the 3D coordination framework, $\{[Cu(in)]\cdot 2H_2O\}_n$, which has an expandable structure that responds to methanol, ethanol and propan-1-ol. The expansion occurs in a spring-like fashion along the channel on guest inclusion and is probably due to rotation of the Cu–O or Cu–N bonds in the ligand [104].

Structural 'breathing' has been observed in interpenetrated and inter-digitated 3D frameworks, and arises from the slipping motion of the interpenetrated layers. The $(ZnI_2)_3(tpt)_2$ framework undergoes considerable relative motion of the two interpenetrating (10,3-*b*) networks during nitrobenzene guest removal and reintroduction with retention of single crystal structure [93]. A reversible sponge-like structural change was observed for $\{[Cu_5(bpp)_8(SO_4)_4(EtOH)(H_2O)_5]\cdot SO_4\cdot EtOH\cdot 25.5H_2O\}_n$, which is probably due to variable ligand conformations and to the flexibility of the catenated architecture [103].

4. Guest-induced responses

Adsorption in the porous structure of classical rigid adsorbents usually involves surface, Knudsen or gas phase diffusion with the importance of the mechanism depending on the size of the porosity. There is an increased attraction in the micropores caused by the overlap of the potential energy surfaces of pore walls. Some materials such as activated carbons may have both hydrophilic functional groups and hydrophobic graphene layer adsorption sites. The porous structures usually range from slit to spherical shapes. In the case of MOFs, pore geometries are more extensive and there may be an increased affinity for adsorption on alternative sites, for example, an increased potential exists at a corner point compared to a flat wall for geometric pores (Fig. 9) [120,121]. This was postulated as the mode of coordination for carbon dioxide adsorption on the $Ni_2(4\text{-}4'bipy)(NO_3)_4$ structure [54], and this is supported by theoretical calculations on $[Cu(bpdc)(DABCO)_{0.5}]_n$, where adsorption is predicted to occur, in two steps, on the two different 'corner' sites[120]. The variation in pore structure may subsequently produce a difference in the adsorption behavior of the adsorbent.

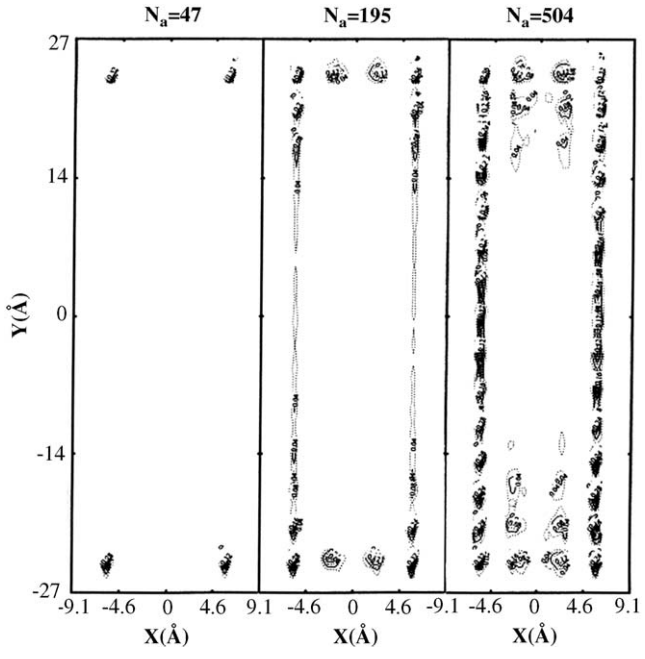

Fig. 9. Contours of constant local density for several values of the pore loading for a cross-section equal to 4×12 Ar atoms. These local densities have been averaged along the direction of the pore axis and thus show where adsorption is occurring in a cross-sectional view down the axis. It is evident that $N_a = 47$ (where N_a is number of atoms) corresponds to a pore where all atoms are adsorbed in the corners of the pore; $N_a = 195$ corresponds to full corners plus partial wall coverage; and $N_a = 504$ corresponds to full corners and walls plus partial filling in the pore center [120].

The IUPAC classification system is based on isotherms that have been obtained for previously studied rigid adsorbent systems. However, the flexibility exhibited by MOFs contradicts this primary assumption of 'rigid' adsorbent studies and a change in adsorption behavior may be observed. There are many examples of variations in framework topology and porous structure, which can be a result of the individual components chosen or the specific interactions that occur between these species or those that arise from their combination. However, it still remains for an understanding of the ability to tailor framework function with molecular assembly. Frameworks that demonstrate flexible structural transformations have been referred to as third-generation materials by Kitagawa [122].

There are two main categories of guest-induced structural distortion; crystal-to-amorphous transformation occurs when the framework collapses upon guest removal but regeneration is possible by guest resorption, or a crystal-to-crystal transformation where guest removal or exchange causes structural change without loss of crystallinity, i.e. unit cell expansion/contraction or scissoring.

Transformations for single crystals have been measured directly by X-ray diffraction [98,119,123]. The systems studied include a 2D net, where smaller channels are extended when adjacent layers 'slide' over each other and align, allowing accommodation of larger guest species [98]. Carbon dioxide forms ordered—1D chains within the void space of evacuated $[Rh(II)_2(O_2CPh)_4(pyz)]_n$ crystals upon cooling in a CO_2 atmosphere, driving a transition from monoclinic to triclinic symmetry [123].

Crystal transformation by guest exchange has been achieved by anion-exchange and the first reversible process was reported in 1996 [124]. An aqueous suspension of crystalline $[Ag(NO_3)(4,4'\text{-bipy})]_n$ is known to undergo a structural transformation in an excess of $NaPF_6$, which is reversible upon addition of KNO_3. Another silver complex, $[Ag(edtpn)(NO_3)]_n$, changes from a 1D structure to 2D layer and box-like networks, upon anion-dependent rearrangement with re-coordination of the Ag(I) center (Fig. 10) [125]. Several other examples have been reported in the literature [107,126–129]. However, the mechanism of anion exchange is not yet fully understood, with a range of dissolution-based processes implied in some cases by detailed AFM studies [130], but the ability to interconvert assemblies widens the scope of structures available for potential applications.

An anticipated property of third-generation materials is the ability to crystallographically transform in response to physical stimuli, including light, magnetic and electric fields as well as for heat (as is commonly observed for other categories of coordination polymers). However, limited transformations for porous materials

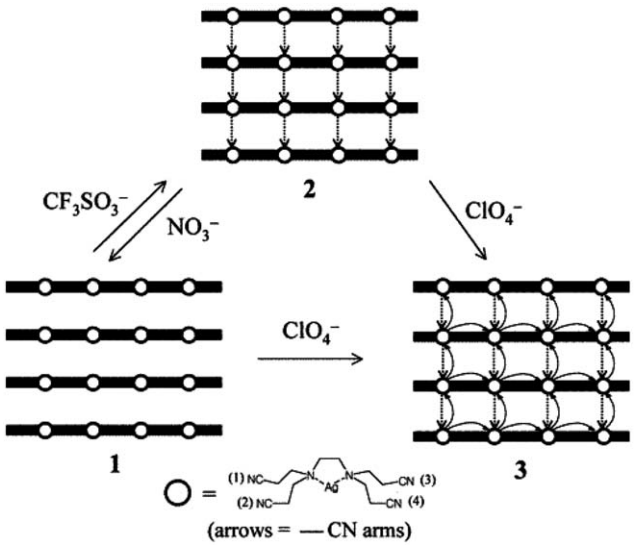

Fig. 10. When the NO_3^- anion in $[Ag(C_{14}H_{20}N_6)(NO_3)]$ is exchanged with $CF_3SO_3^-$, the linear chains of $[Ag(C_{14}H_{20}N_6)(NO_3)]$ are linked together by using one of the three free cyano groups of an EDTPN that coordinates a Ag(I) ion of the neighboring chain, which gives rise to a 2D layer of $[Ag(C_{14}H_{20}N_6)]CF_3SO_3$. When the $CF_3SO_3^-$ anion is exchanged with NO_3^-, the cyano groups linking the 1D chains are dissociated. When the $CF_3SO_3^-$ anion of $[Ag(C_{14}H_{20}N_6)]CF_3SO_3$ is exchanged with ClO_4^-, two free cyano groups of an EDTPN in $[Ag(C_{14}H_{20}N_6)]CF_3SO_3$ bind two neighboring Ag(I) ions, one in its own chain and the other in the adjacent chain, which leads to the box-like 2D structure of $[Ag(C_{14}H_{20}N_6)]ClO_4$. When the NO_3^- anion in $[Ag(C_{14}H_{20}N_6)(NO_3)]$ is exchanged with the ClO_4^- anion, three free cyano groups of $[Ag(C_{14}H_{20}N_6)(NO_3)]$ bind three Ag(I) ions, one Ag(I) ion in its own chain and two Ag(I) ions in two different neighboring chains, which gives rise to the structure of $[Ag(C_{14}H_{20}N_6)]ClO_4$. According to this scheme, the structural transformations among $[Ag(C_{14}H_{20}N_6)(NO_3)]$, $[Ag(C_{14}H_{20}N_6)]CF_3SO_3$ and $[Ag(C_{14}H_{20}N_6)]ClO_4$ are possible in the crystalline state, just by the coordination or uncoordination of polynitrile arms of the ligand without significant changes of the location of Ag(I) ions and edtpn ligands [125].

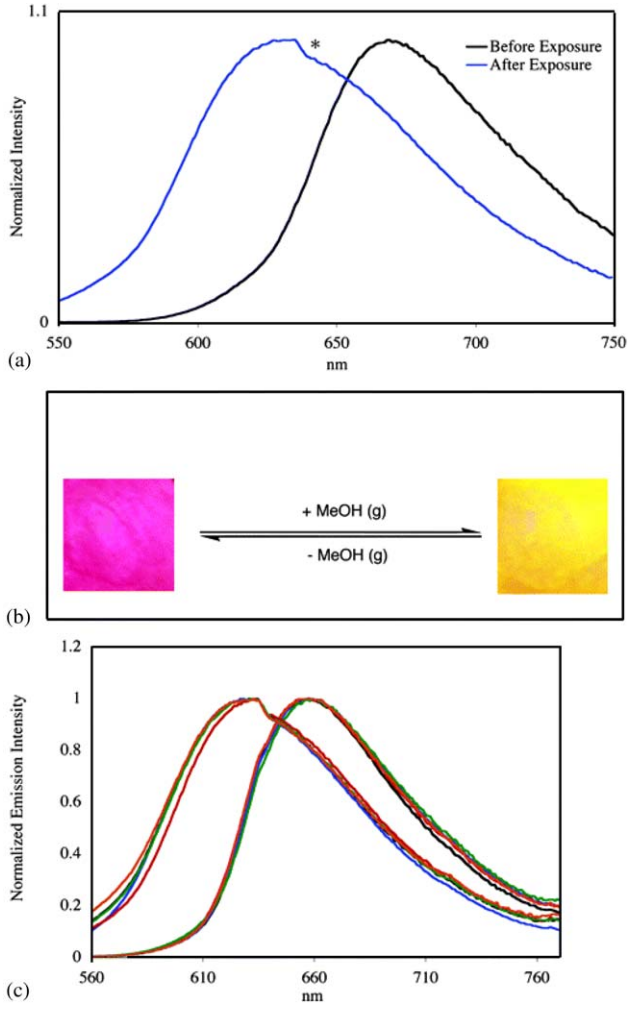

Fig. 11. (a) Normalized room-temperature solid-state emission spectrum of $[Pt(Nttpy)Cl](PF_6)_2$ before and after exposure to MeOH vapors. *Denotes instrumental artifact. (b) Luminescence of $[Pt(Nttpy)Cl](PF_6)_2$ as observed by eye in the presence and absence of MeOH vapors. The complex is immobilized on filter paper and irradiated under long-wave UV-light at room temperature. (c) Emission results obtained from cycling through repeated exposure to and removal of MeOH vapor in air [131].

have been reported in the literature. $[Pt(Nttpy)Cl](PF_6)_2$ is brightly luminescent in the solid state at room temperature and 77 K. Exposure to certain volatile organic solvents produces a reversible crystallographic change, for example, methanol invokes a vapochromic change where the color changes from red to orange (Fig. 11). The X-ray diffraction of the same single crystal of the two forms showed equivalence molecularly (distorted square planar) with a small change in packing. The main difference is the presence of solvent molecules in lattice voids for only the orange form [131]. Diffraction patterns of $\{[Cu_2(pzdc)_2(4,4'\text{-bipy})]G\}$, (CPL-2 G) where $G = H_2O$ or benzene, or $G =$ void for the apohost, were measured using in situ synchrotron X-ray powder diffraction. Benzene adsorption induced a crystallographic contraction, with ~4.9% reduction in volume, even though the channels were occupied by benzene. The transformation produces a new pore structure that is well suited for benzene, which the authors call a 'shape-responsive fitting transformation' [132]. Examples also exist for inorganic mesoporous silica MCM-41 [133,134], and it is envisaged that third-generation materials that respond to physical stimuli will be discovered allowing a greater diversity in the materials available for study.

Reversible adsorption characteristics and electronic switching, sensitive to guest species, have been observed for $Fe_2(azpy)_4(NCS)_4 \cdot$(guest). The switching property is due to iron(II) spin crossover centers, where 'half-spin' crossovers are produced in the sorbed phase and no switching upon desorption. The local environment of the iron(II) centers changes with adsorption, due to the structural flexibility of the framework, which shows

dramatic changes in geometry with sorption. The theoretical basis proposed may have important implications in molecular sensing [8].

NMR has been used to study the polymeric complex, $[Ni(4,4'\text{-bipy})(DBM)_2]$, which adsorbs large volumes of gases/VOCs, as suitable single crystals could not be grown for X-ray analysis. Adsorption of xenon produces a Type-I isotherm, with a plateau value of 1:2 (host-to-xenon). Adsorption of organic vapors produces structural changes, ranging from minor adjustments to total reorganization of the crystal structure. NMR studies with benzene-*d*6 showed that the organic molecule is included in the crystalline lattice of the parent material [135].

4.1. Step changes

An example is the adsorption of methanol on the **E** polymorph of $Ni_2(4\text{-}4'\text{-bipy})(NO_3)_4$. Readsorption of the templating molecule (EtOH) produces a Type-I isotherm, indicative of the microporous structure present. However, substitution by methanol causes a change in structure as the flexible adsorbent expands in order to accommodate three methanol molecules into the void originally occupied by two ethanol molecules (see Fig. 12). The structural rearrangement, which results in the net cell expansion, produces a step in the isotherm at volume filling equal to a formula stoichiometry of two methanol molecules, with a scissoring motion involving an increase in two axes and a reduction in the third allowing a third methanol molecule to be sorbed. This change is accompanied by a slowing down of the sorption kinetics. The structural change is forced by the precise optimization of the **E** structure around the ethanol template, which occupies the cavity shown in Fig. 2(d): there are two ethanol guests per formula unit in the as-grown material, and thus **E** is optimized for hydrogen bonding two hydroxyl groups. When the third methanol guest per formula unit is sorbed, the structure is forced to readjust to accommodate it, producing both the isotherm step and the slow kinetics at this point [54].

4.2. 'Gating' processes

This may occur when the porous structure of a material changes during the adsorption process, going from non-porous to porous at a specific pressure and generating an isotherm that could be the combinatorial result of two or more types. The adsorption isotherm obtained for a $\{[Co(NCS)_2(4\text{-peia})_2]\cdot 4Me_2CO\}_n$ shows an apparent change in structural character from non- to microporous at a set pressure as shown in Fig. 13 [136]. The isotherm is similar to Type II at low pressure, and the low uptake is consistent with a lack of porosity, however, at $p/p^0 \sim 0.75$ there is a sharp increase in uptake with Type-I character, indicative of a microporous structure. Once the plateau is reached the structural change is complete and the porous structure is filled with guest molecules. Other systems may produce isotherms where a progressive opening of the porosity, which may be composed of different pore widths, will produce stepped isotherms.

Adsorption studies of nitrogen, argon and carbon dioxide on $[Cu(4,4'\text{-bipy})(BF_4)(H_2O)_2\cdot(4,4'\text{-bipy})]_n$, produced an adsorption profile that again showed a sharp increase in mass at a given pressure, referred to by the authors as the 'gate pressure'. Almost no adsorption was observed below this pressure and the change was attributed to pore blocking below the 'gate pressure' by hydrogen bonds, which regulate the microporous nature of the adsorbent [102].

Flexibility of coordination polymer frameworks has been exploited to activate access to the porosity using the guest pressure. This exploits either freedom to displace one interpenetrated network relative to another or uses the guest pressure to overcome the weakest framework-forming interaction in a low-dimensional system [114]. $[Cu(4,4'\text{-bipy})(dhbc)_2]\cdot H_2O$ is stable to guest loss but the interlayer separation decreases to prevent nitrogen adsorption at 77 K. However, the nitrogen sorption isotherm, at 300 K, demonstrates an abrupt increase in uptake beyond ~50 bar, referred to as the 'gate-opening' pressure, which corresponds to a structural transition from the 'closed' to the 'open' form driven by interaction between the framework and the guest (Fig. 14). The lanthanide-based carboxylate framework $Er_2(pda)_3$ behaves as though it has microporosity for carbon dioxide adsorption at 273 K but not argon or nitrogen adsorption at 77 K. The authors suggest that chemical rather than size factors control guest uptake into the porosity [137]. However, activated diffusion effects are also possible for adsorption in microporous structures at 77 K [138,139].

4.3. Gas storage

Storage of selected gases or vapors is a desirable characteristic of porous materials. Particularly important is the storage of hydrogen and methane at ambient temperatures and relatively low pressures for use in transportation applications. Materials with such ability need to include an extended porous structure and pore volume. In the case of porous MOFs, they must retain a stable accessible void for gas adsorption after evacuation.

Methane: Classic rigid adsorption systems, such as activated carbon, have reasonable methane storage capacity but limited commercial feasibility, due to distance limitations for refueling; to date up to ~150 v/v (~270 $cm^3\,g^{-1}$) uptakes have been achieved, at 35 bar and 298 K, which actually meet the targets set by the US DoE. The volume of methane adsorbed per

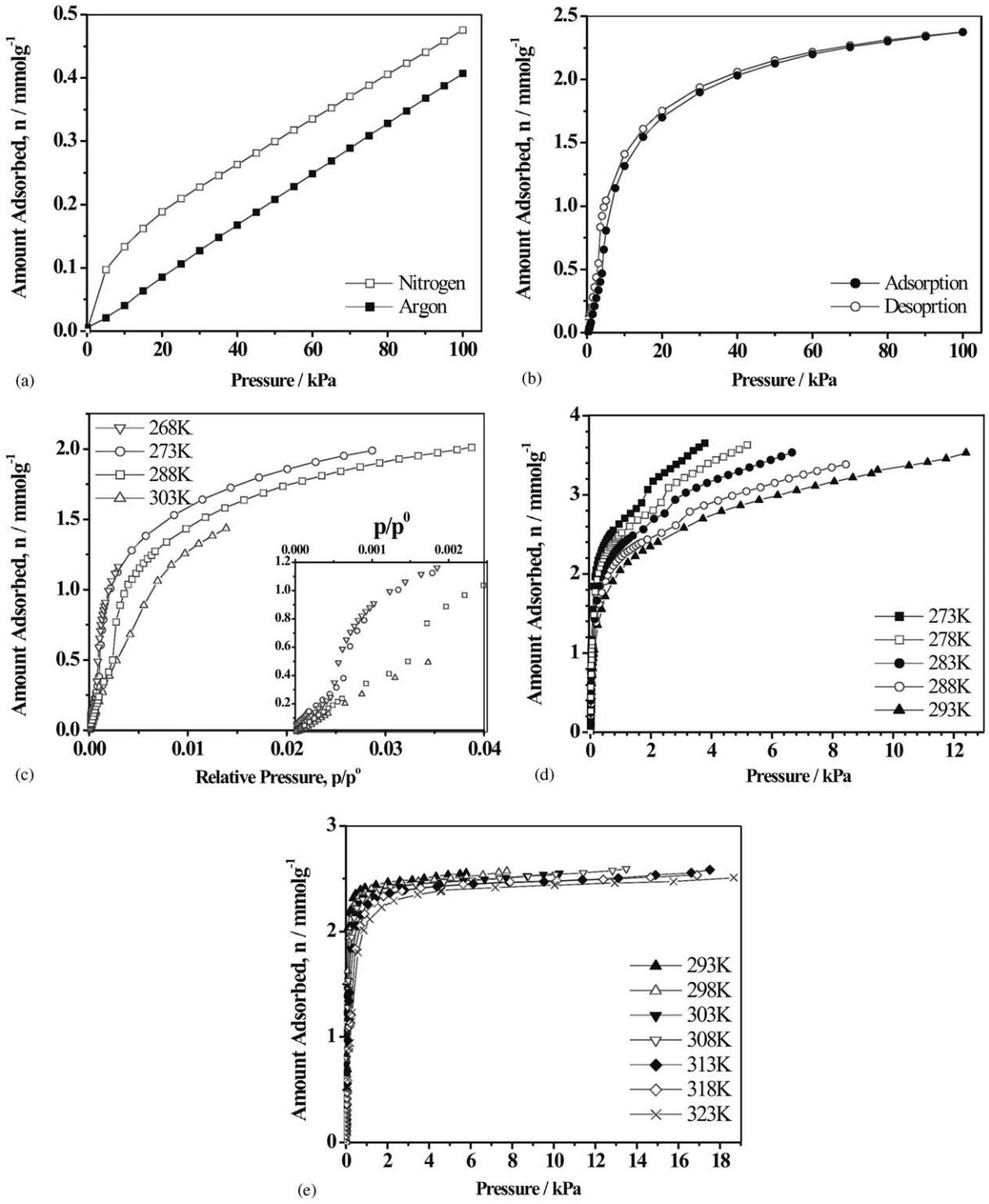

Fig. 12. (a) Adsorption isotherms for nitrogen and argon on $Ni_2(4,4'\text{-bipyridine})_3(NO_3)_4$ at 273 K. (b) Adsorption/desorption isotherms for nitrous oxide $Ni_2(4,4'\text{-bipy})_3(NO_3)_4$ at 273 K. (c) Adsorption isotherms for carbon dioxide on $Ni_2(4,4'\text{-bipy})_3(NO_3)_4$ in the temperature range 268–303 K and pressure range p/p^0, 0–0.04 (p/p^0, 0–0.0025, inset). (d) Adsorption isotherms for methanol on $Ni_2(4,4'\text{-bipy})_3(NO_3)_4$ in the temperature range 273–293 K. (e) Adsorption isotherms for ethanol on $Ni_2(4,4'\text{-bipyridine})_3(NO_3)_4$ in the temperature range 293–323 K [54].

volume of adsorbent is the most important factor in determining commercial viability. One of the problems is that the presence of meso- and macropores does not contribute greatly to methane adsorption capacity, as the pores are too wide for pore filling under the adsorption conditions. However, the advantage of materials with a pore size distribution like activated carbons is that it improves gas adsorption/desorption

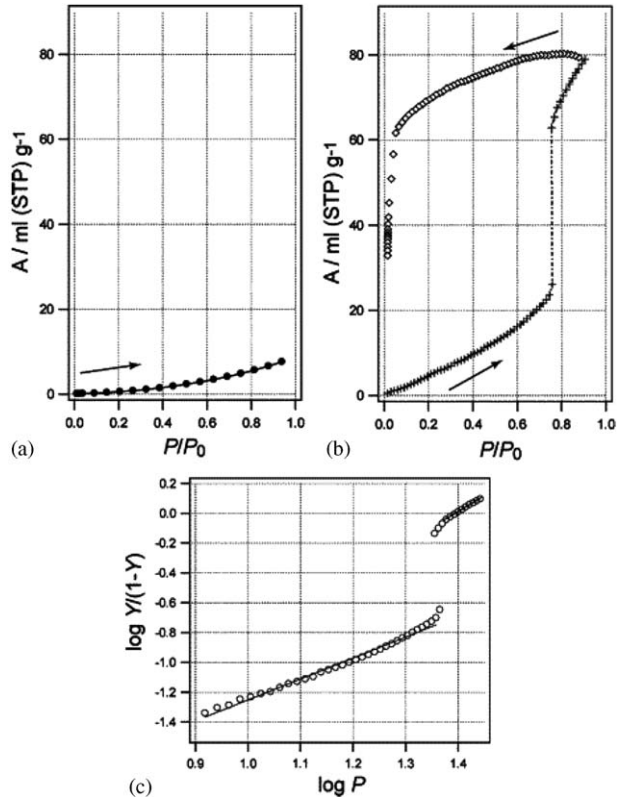

Fig. 13. (a) Isotherm for N_2 adsorption (filled circles) at 77 K of $\{[Co(NCS)_2(4\text{-peia})_2]\cdot 4Me_2CO\}_n$ over the pressure range from 0.003 to 0.919. P_0 is the saturated vapor pressure of N_2 at 77 K. (b) Isotherm for acetone vapor adsorption (crosses) and desorption (open squares) at 298 K of $[Co(NCS)_2(4\text{-peia})_2]$ over the relative pressure range 0.017 to 0.907. (c) Hill plot for the adsorption curve of (b), where Y ($0<Y<1$) and P are the extent of complexation and pressure (kPa), respectively [136].

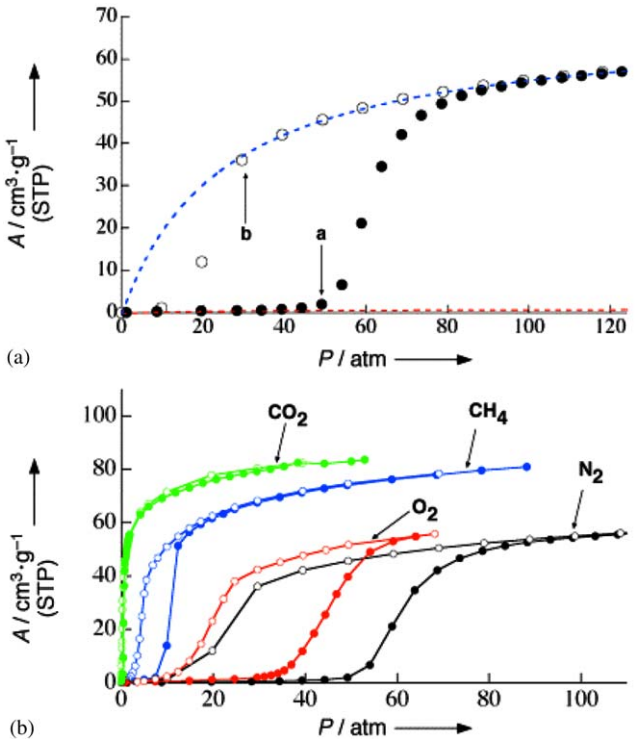

Fig. 14. (a) Nitrogen adsorption (filled circles) and desorption isotherms (open circles) for $[Cu(4,4'\text{-bipy})(dhbc)_2]\cdot H_2O$ at 298 K. Blue and red dashed lines were determined by fitting the linear parts of the Langmuir plots in the higher (from 82 to 121 bar) and lower (from 8 to 33 bar) pressure ranges, respectively. (b) Adsorption (filled circles) and desorption (open circles) isotherms of N_2, CH_4, CO_2 and O_2 at 298 K [114].

transport characteristics. This is a scenario where tailored pores, with pore widths close to the adsorbate dimensions, are a possible more-expensive alternative and an area where MOFs may potentially provide molecules with improved capacity, due to the uniform porosity with large pore volume.

The first report of using MOFs for methane adsorption was made in 1997 [51] for the polymeric material $\{[Co_2(4,4'\text{-bipy})_3(NO_3)_4]\cdot 4H_2O\}_n$. The adsorbent sorbs $\sim 52\,cm^3\,g^{-1}$ at ambient temperature and ~ 30 bar pressure (Fig. 15). Further investigations on $\{[Cu_2(pzdc)2L]\cdot nH_2O\}_n$ (L = pyz (CPL-1, $n=1$), 4,4′-bipy (CPL-2, $n=4$), and pia (CPL-6, $n=5$)) [28] have shown uptakes of 18, 56 and 65 $cm^3\,g^{-1}$ of methane under similar conditions. A variety of porous frameworks have been synthesized since this initial report, which display similar adsorption characteristics [17,19,39,46,48,49,53,55,56,58,89,101,102,140–143].

Interpenetrated frameworks have also exhibited sorption of methane, the first example being 40 $cm^3\,g^{-1}$ at 298 K and 35 bar for $\{[Cd_2(NO_3)_4(azpy)_3]\cdot 2Me_2CO\}_n$, which has a microporous structure despite being a triply interpenetrated framework [140]. Later structures have produced increased capacities: $\{[Cu(AF_6)(4,4'\text{-bipy})_2]\cdot 8H_2O\}_n$ (when A = Si, $V_{ads} = 134\,cm^3\,g^{-1}$; and A = Ge, $V_{ads} = 146\,cm^3\,g^{-1}$), again at 298 K and 35 bar [19,89], suggesting that improved design of MOFs may provide viable storage materials in future.

The isoreticular metal-organic frameworks (IRMOFs) related to MOF-5 exhibit an increased capacity towards methane. One particular material, an isoreticular $Zn_4O(O_2CR)_6$ framework with cyclobutylbenzene linkers; IRMOF-6, with a large surface area ($2630\,m^2\,g^{-1}$) [46] shows an uptake of 240 $cm^3\,g^{-1}$ at 35 bar and 298 K. This equates to ~70% of the volume that is currently stored in gas tanks, which use greater pressure (>200 bar).

Other porous polymers, composed of 2D carboxylate-bridged polymers bridged by organic linkers to produce a 3D network [142], show large methane uptakes ($\sim 212\,cm^3\,g^{-1}$ at 298 K and 34 bar), which may be supported by their relatively large surface areas (in the region of $3200\,m^2\,g^{-1}$) or channel cross-sectional size. These authors suggest that an upper limit of

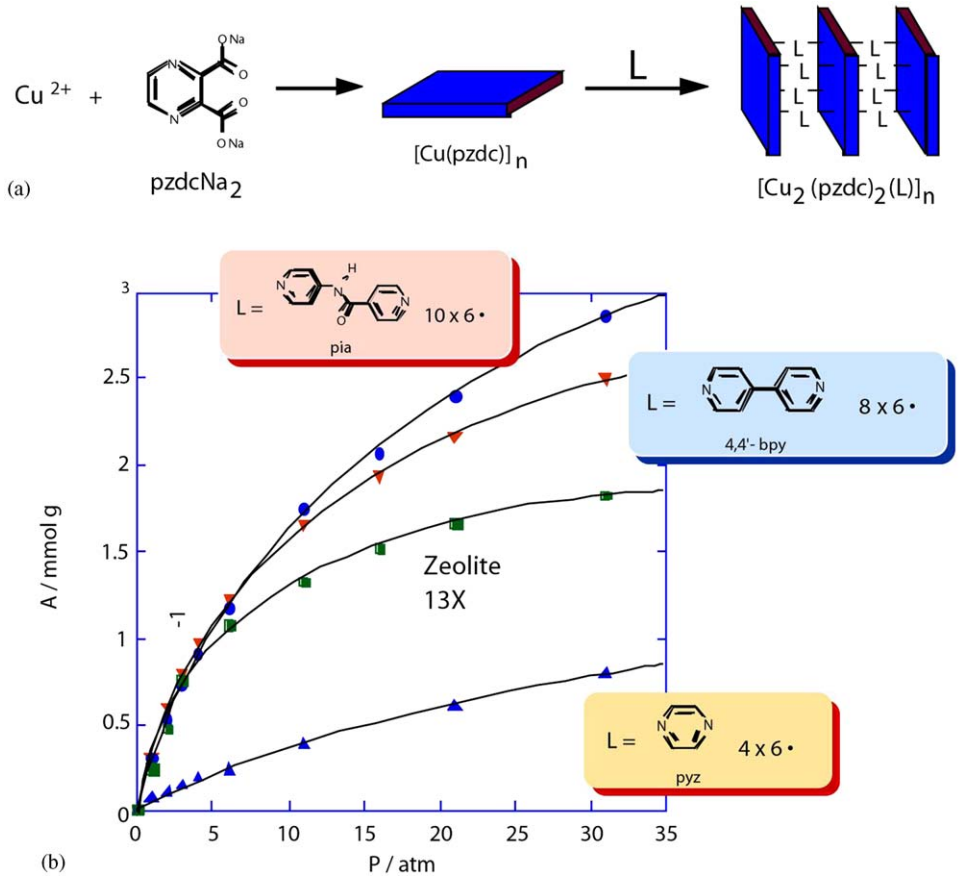

Fig. 15. Adsorption isotherms for $\{[Cu_2(pzdc)_2(pyz)]\cdot 2H_2O\}_n$, $\{[Cu_2(pzdc)_2(4,4'\text{-bipy})]\cdot 5H_2O\}_n$ and $\{[Cu_2(pzdc)_2(pia)]\cdot 5H_2O\}_n$ obtained with CH_4 between 1 and 35 bar. A = Absolute adsorption (mmol g^{-1}) [28].

$\sim 12 \times 12\,\text{Å}^2$ probably exists for square pores in methane storage applications, where maximum potential interaction between the adsorbate and adsorbent would occur, implying that simply further increases in pore dimensions will not improve performance.

Hydrogen: The environmental implications of replacing petrol- and diesel-powered transportation by versions that run on fuel cells and hydrogen have gained much media interest in recent years. The main benefits of using this 'clean fuel' are massive reductions in air pollution and greenhouse gas emissions, and this has led to a great surge in research into efficient storage of the gas. Current methods of hydrogen storage are themselves energy intensive, requiring cryogenic temperatures, whilst hydrogen-powered transportation will require great advances in storage methods for use with fuel cells necessary to convert the fuel to power. Hence, there is a need to develop adequate storage materials in conjunction with vehicular technology that are able to store large amounts of hydrogen at near-ambient temperatures and 'safe' pressures. Such materials would also need to satisfy the requirements of reasonable volume, weight and realistic kinetics for charging and discharging the gas.

Firstly, it is important to point out that there have been a number of erroneously high hydrogen adsorption uptakes reported for both carbons and MOFs. Accurate hydrogen adsorption measurements are difficult and many of the problems are associated with the adsorption of impurities in the hydrogen used. Few papers contain sufficient information to cross check the reasonableness of the adsorption uptakes against standard pore structure characteristics, as obtained from nitrogen (77 K) and carbon dioxide (273 K) adsorption studies, e.g. confirmation that the pore volumes for hydrogen uptake are not greater than possible from the total pore volume determined by nitrogen sorption.

The United States Department of Energy has current targets of 6.0 wt% for hydrogen storage by the year 2010 [144]. This means that given the energy density of hydrogen compared to petrol and the projected increased efficiency of fuel cells over the combustion engine, an average vehicle would require 5–10 kg of hydrogen to be stored for equivalent transportation [145]. Nijkamp et al. [146] proposed that a correlation exists between hydrogen volume adsorbed and micropore volume by deconvoluting the amounts adsorbed in the micropores and the surface of the micropores for

carbons. This allowed the authors to conclude that greater gas capacities could be achieved with adsorbents containing a large volume of micropores with suitable diameter [146]. Recent work involving the investigation of the effect of carbon surface functionality on hydrogen adsorption showed a clear correlation between the maximum volume of hydrogen adsorbed and micropore volume, determined from extrapolation of the Dubinin–Radushkevich equation for carbon dioxide adsorption at 273 K, and suggest that only the micropore volume is filled with hydrogen at 77 K [147]. The micropore volume can be converted to a surface area and, hence, shows consistency with the correlation between hydrogen adsorption and surface area observed previously [148]. The work by Zhao et al. also suggests that the effect of functional groups is detrimental to hydrogen adsorption on activated carbons. Isobars for hydrogen adsorption show a decrease in amount of hydrogen adsorbed with increasing temperature from 77 K with the amount adsorbed becoming negligible at 195 K [147]. Initial studies [149–151] of hydrogen adsorption on graphitic fibers, carbon nanotubes and porous carbons showed high uptakes but recent work has questioned earlier observations [146,152–156]. The temperature dependence of hydrogen adsorption is a major consideration for the use of adsorbents. Current carbon adsorbents only take up small amounts of hydrogen adsorption even at high pressures (up to 100 bar) [154–158], which has also been suggested by theoretical calculations [159–161]. Even considering the most efficient carbon adsorbent as a pure graphitic sheet with complete adsorption on both sides, adsorption capacities are limited.

Previous work has focused largely on metal hydrides [145,162,163], which involves chemisorption where the issues of low storage capacity or high-release temperature may need addressing, while the important process for zeolites [164], and carbon-based (including nanotubes) [149,150,165–172] materials is physisorption. There is also the development of chemical hydrides with catalyst doping, e.g. Ti-doped $NaAlH_4$, which have been shown to reversibly cycle hydrogen [173,174]. The major disadvantage of using hydrides for hydrogen storage is the large enthalpy generated during adsorption, which presents a problem when refueling a vehicle at the rate proposed by the US DoE.

Recent work involves the use of MOF-177; $Zn_4O(BTB)_2$ [40] IRMOFs-1, -8, -11 [46], and -18 [175]; these are $Zn_4O(O_2CR)_6$ IRMOFs having bdc, ndc, hpdc and tmbdc linkers, respectively. The microporous coordination polymers show adsorption of hydrogen up to 1.6 wt% at 77 K and ~1 bar pressure for IRMOF-11 [171]. IRMOF-1 has also been shown to adsorb ~1.65 wt% at room temperature and 48 bar [176]. Panella et al. [177] have recently reported that hydrogen adsorption studies on MOF-5 (also known as IRMOF-1) at room temperature and at 77 K for pressures between 1 and 67 bar show good agreement with the newer values reported by Roswell et al. [175] in 2004 for the IRMOF series. These authors also reported that the material exhibits a very small uptake at room temperature, even up to 67 bar, at 0.2 wt%. Zhao et al. [37] have presented isobar data, which show that negligible amounts of hydrogen were adsorbed on activated carbon and MOFs at 195 K and 1 bar hydrogen. Given the well-defined porous structure of many MOF and inorganic porous systems, information on which sites within the structure specifically favor hydrogen adsorption will be useful in developing new classes of material. Temperature-programmed desorption and inelastic neutron scattering measurements suggest that the nickel(II) phosphate VSB-5 has coordinatively unsaturated Ni^{II} sites accessible to hydrogen molecules in the pores [178], which may enhance adsorption. Interpenetrating materials may need to be an aspect to consider in the design of MOFs to produce a suitable porous structure of hydrogen adsorption [175].

Ferey et al. [179] describe hydrogen adsorption on $M(OH)(O_2C–C_6H_4–CO_2)$, where $M = Cr^{3+}$ or Al^{3+}. Fig. 16 shows that significant adsorption was observed. The chromium material shows an uptake of 3.1 wt% (at 1.6 MPa) [179,180], whereas that containing aluminum shows 3.8 wt% [179,181] at the same pressure. Hysteresis was observed for adsorption of hydrogen on the two compounds. Comparison with other rigid systems shows a greater capacity for hydrogen gas at 77 K but no significant hydrogen uptake is observed at room temperature [179] Selective adsorption of hydrogen (0.9 wt%) over nitrogen, at 78 K, has been demonstrated for a MOF with short linkers [182]. However, the low temperatures used suggest activated diffusion effects

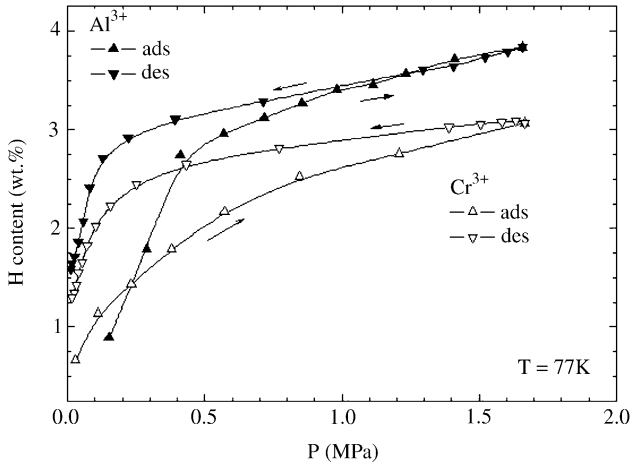

Fig. 16. PCI curves (▲: adsorption; ▼: desorption) measured at 77 K up to 1.6 MPa of hydrogen pressure for $M(OH)(O_2C–C_6H_4–CO_2)$ samples with $M = Cr^{3+}$ (open symbol) and $M = Al^{3+}$ (full symbol) [179].

should be considered. Other authors have reported uptakes of a few percent for adsorption at ~1 bar and 77 K; [Ni (cyclam)(bpydc)] showed 1.1 wt% [34], while the zinc-based framework $[Zn_2(bdc)_2(DABCO)]$ [38] had an uptake of 2.0 wt% both of which would be expected to be very much lower at room temperature.

The adsorption of large volumes of hydrogen is inherently difficult due to the small molecular dimensions of the molecule and the limited interactions between the adsorbent, either classical rigid materials or MOFs, and poorly polarizable hydrogen molecules. This leads to a marked temperature dependence for hydrogen physisorption with little or no hydrogen being adsorbed at 195 K and 1 bar. It is not sufficient to make increasingly large pore volumes with large pores, as a surface potential well overlap is critical for hydrogen adsorption. Hence, the production of materials that incorporate small pores, preferably specifically designed to maximize hydrogen sorption via the nature and spatial distribution of functional groups, or large pores with windows that can retain the adsorbate are the most reasonable approaches available.

4.4. *'Kinetic trapping'*

Physical adsorption of species on many porous materials produces adsorption isotherms that are virtually completely reversible. A recent report [37] has shown that adsorption will produce an effect in the system whereby some or all of the hydrogen is retained on pressure reduction and this is described by the term 'kinetic trapping'.

Studies have shown that adsorption and desorption of hydrogen from nanoporous materials, such as activated carbon, is usually fully reversible [146,183–187] as would be expected for the weak van der Waals-type interactions involved in physisorption processes of this type. However, adsorption of hydrogen on nanoporous MOFs, two structures with $Ni_2(4\text{-}4'\text{-bipy})(NO_3)_4$ stoichiometry (Fig. 2) reveals irreversibility in hydrogen uptake at 77 K. The existence of flexible linkers, weak as well as strong framework-forming interactions and windows, which are considerably smaller than the cavities they connect, may all be important in the process of kinetic trapping of hydrogen gas by windows [37]. The pore openings, as characterized in the static structures, appear to be too small to allow hydrogen (kinetic diameter 2.89 Å) to pass, but there are subtle changes within the structure that allow the gas to access the internal porous structure. Hysteresis in the adsorption and desorption isotherms is observed (Fig. 17), above the supercritical temperature of hydrogen, which reflects the dynamical opening of the windows between pores. The effect of this is to be able to store in the material at reduced pressures concentrations of hydrogen, which are loaded at considerably higher pressures.

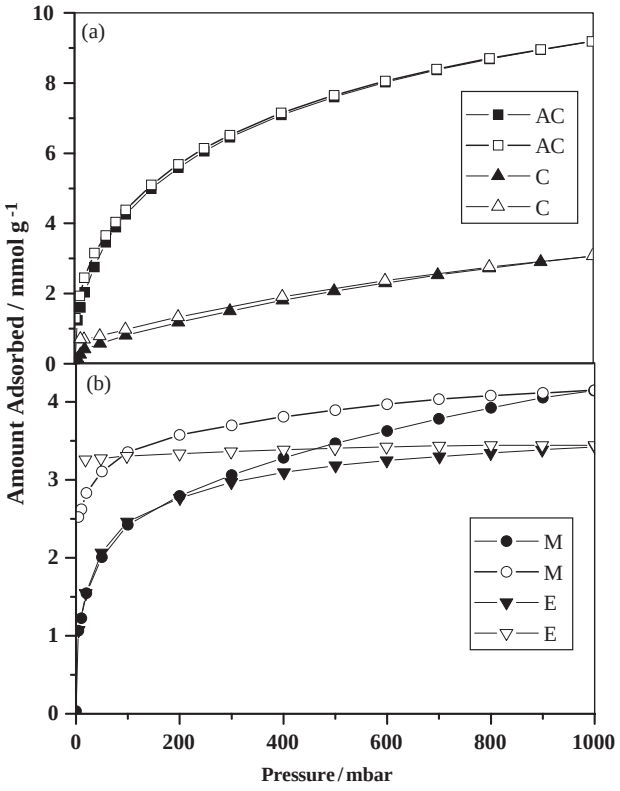

Fig. 17. Adsorption–desorption isotherms for H_2 adsorption (filled symbols) and desorption (open symbols) isotherms on adsorbents at −196 °C: (a) **AC**—activated carbon G209 (■, □), C—$Ni_3(btc)_2(3\text{-pic})_6(pd)_3$ (▲, △); (b) **M** polymorph of $Ni_2(4,4'\text{-bipy})_3(NO)_4$ (●, ○), **E** polymorph of $Ni_2(4,4'\text{-bipy})_3(NO)_4$ (▼,▽) [37].

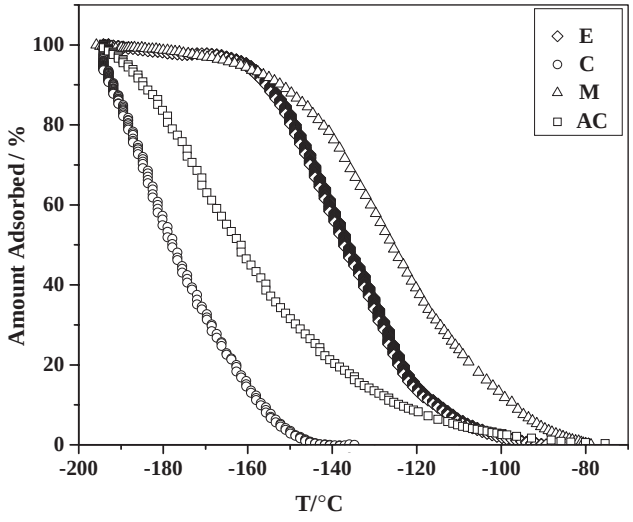

Fig. 18. Isobars for hydrogen desorption from adsorbents; **AC**—activated carbon G209 (□), **E** polymorph of $Ni_2(4,4'\text{-bipy})_3(NO)_4$ (◇), **M** polymorph of $Ni_2(4,4'\text{-bipy})_3(NO)_4$ (△) and **C**—$Ni_3(btc)_2(3\text{-pic})_6(pd)_3$ (○) at 1 bar hydrogen pressure [37].

The hydrogen gas can be stored at 77 K and its release starts at 110 K, which is complete when the temperature reaches 195 K, as shown by measured isotherms

(Fig. 18). The isobars contrast with the "reversible" systems (activated carbons, rigid adsorbents and MOFs without windows) in that there is virtually no loss of mass on heating between 77 and 110 K, demonstrating that the systems are not at equilibrium. This behavior is quite different from rigid adsorbents such as activated carbons. The unique behavior demonstrated by these materials would allow hydrogen to be adsorbed at high pressures but stored at lower pressures. The challenge is to increase the temperature at which release of hydrogen starts. Given that this is determined kinetically by an activation barrier, it may well be possible to raise this barrier by modification of the structure or interactions within it controlling the window opening and closing.

5. Conclusions and future perspectives

Studies of gas/vapor adsorption characteristics of adsorbents provide information that allows tailoring of properties for potential applications. This is of particular interest in the field of porous coordination materials, where the pore cavity size and shape, and window structure available may be controlled by rational design for a specific application.

Specific differences between MOFs and classical rigid adsorbents are related to the flexibility of the former. Structural changes, for example, a scissoring motion, may occur during the adsorption process. Rigid adsorbents may frequently follow Gurvitsch's rule, whereas MOFs often do not. This is related to the presence of pore cavities, which may control adsorption in MOFs. Flexibility is also needed to allow opening/closing of windows in the structure to provide access to the pore structure. 'Gating' and 'kinetic trapping' processes are unique to flexible MOFs. Disadvantages of these systems compared to classical adsorbents, such as activated carbons and zeolites, including lower thermal and chemical stability of MOFs, must be balanced against the rational design process for tailoring structures to specific properties.

References

[1] O.M. Yaghi, M. O'Keeffe, N.W. Ockwig, H.K. Chae, M. Eddaoudi, J. Kim, Nature 423 (2003) 705–714.
[2] S. Kitagawa, R. Kitaura, S.-I. Noro, Angew. Chem. Int. Ed. 43 (2004) 2334–2375.
[3] B. Moulton, M.J. Zaworotko, Curr. Opin. Solid State Mater. Sci. 6 (2002) 117–123.
[4] R. Robson, J. Chem. Soc. Dalton Trans. (2000) 3735–3744.
[5] G.A. Mines, B.-C. Tzeng, K.J. Stevenson, J. Li, J.T. Hupp, Angew. Chem. Int. Ed. 41 (2002) 154–157.
[6] S.-S. Sun, A.J. Lees, J. Am. Chem. Soc. 122 (2000) 8956–8967.
[7] S.J. Lee, W. Lin, J. Am. Chem. Soc. 124 (2002) 4554–4555.
[8] G.J. Halder, C.J. Kepert, B. Moubaraki, K.S. Murray, J.D. Cashion, Science 298 (2002) 1762–1765.
[9] M.L. Merlau, M. del Pilar Mejia, S.T. Nguyen, J.T. Hupp, Angew. Chem. Int. Ed. 40 (2001) 4239–4242.
[10] K.E. Splan, A.M. Massari, J.T. Hupp, J. Phys. Chem. B 108 (2004) 4111–4115.
[11] K.F. Czaplewski, J.T. Hupp, R.Q. Snurr, Adv. Mater. 13 (2001) 1895–1897.
[12] L. Huang, H. Wang, J. Chen, Z. Wang, J. Sun, D. Zhao, Y. Yan, Micropor. Mesopor. Mater. 58 (2003) 105–114.
[13] Q.M. Wang, D. Shen, M. Bulow, M.L. Lau, S. Deng, F.R. Fitch, N.O. Lemcoff, J. Semanscin, Micropor. Mesopor. Mater. 55 (2002) 217–230.
[14] K. Schlichte, T. Kratzke, S. Kaskel, Micropor. Mesopor. Mater. 73 (2004) 81–88.
[15] P. Zwietering, D.W. van Krevelen, Fuel 33 (1954) 331–337.
[16] F.A.P. Maggs, Res. Correspondence 6 (1953) S13–S14.
[17] H. Li, M. Eddaoudi, M. O'Keeffe, O.M. Yaghi, Nature 402 (1999) 276–279.
[18] S. Subramanian, M.J. Zaworotko, Angew. Chem. Int. Ed. 34 (1995) 2127–2129.
[19] S.-I. Noro, S. Kitagawa, M. Kondo, K. Seki, Angew. Chem. Int. Ed. 39 (2000) 2081–2084.
[20] L. Carlucci, G. Ciani, D.M. Proserpio, A. Sironi, Angew. Chem. Int. Ed. 34 (1995) 1895–1898.
[21] C. Serre, F. Millange, S. Surble, G. Férey, Angew. Chem. Int. Ed. 43 (2004) 6285–6289.
[22] G. Férey, C. Serre, C. Mellot-Draznieks, F. Millange, S. Surble, J. Dutour, I. Margiolaki, Angew. Chem. Int. Ed. 43 (2004) 6296–6301.
[23] T.J. Prior, D. Bradshaw, S.J. Teat, M.J. Rosseinsky, Chem. Commun. 4 (2003) 500–501.
[24] S.K. Chawla, M. Arora, K. Naettinen, K. Rissanen, J.V. Yakhmi, Polyhedron 23 (2004) 3007–3019.
[25] S.R. Batten, B.F. Hoskins, R. Robson, J. Am. Chem. Soc. 117 (1995) 5385–5386.
[26] K. Biradha, Y. Hongo, M. Fujita, Angew. Chem. Int. Ed. 39 (2000) 3843–3845.
[27] J. Sun, L. Weng, Y. Zhou, J. Chen, Z. Chen, Z. Liu, D. Zhao, Angew. Chem. Int. Ed. 41 (2002) 4471–4473.
[28] M. Kondo, T. Okubo, A. Asami, S.-I. Noro, T. Yoshitomi, S. Kitagawa, T. Ishii, H. Matsuzaka, K. Seki, Angew. Chem. Int. Ed. 38 (1999) 140–143.
[29] S. Kitagawa, R. Kitaura, Comment Inorg. Chem. 23 (2002) 101–126.
[30] W.J. Belcher, C.A. Longstaff, M.R. Neckenig, J.W. Steed, Chem. Commun. 15 (2002) 1602–1603.
[31] K. Biradha, M. Fujita, J. Inclusion Phenom. 41 (2001) 201–208.
[32] C.-Y. Su, A.M. Goforth, M.D. Smith, H.-C. zur Loye, Chem. Commun. 19 (2004) 2158–2159.
[33] Y. Zou, W.-L. Liu, C.-S. Lu, J.-L. Xie, C.-L. Ni, Q.-J. Meng, Inorg. Chem. Commun. 6 (2003) 1217–1219.
[34] E.Y. Lee, M.P. Suh, Angew. Chem. Int. Ed. 43 (2004) 2798–2801.
[35] O.M. Yaghi, G. Li, H. Li, Nature 378 (1995) 703–706.
[36] D. Bradshaw, T.J. Prior, E.J. Cussen, J.B. Claridge, M.J. Rosseinsky, J. Am. Chem. Soc. 126 (2004) 6106–6114.
[37] X. Zhao, B. Xiao, A.J. Fletcher, K.M. Thomas, D. Bradshaw, M.J. Rosseinsky, Science 306 (2004) 1012–1015.
[38] D.N. Dybtsev, H. Chun, K. Kim, Angew. Chem. Int. Ed. 43 (2004) 5033–5036.
[39] S.S.-Y. Chui, S.M.-F. Lo, J.P.H. Charmant, A.G. Orpen, I.D. Willaims, Science 283 (1999) 1148–1150.
[40] H.K. Chae, D.Y. Siberio-Perez, J. Kim, Y. Go, M. Eddaoudi, A.J. Matzger, M. O'Keeffe, O.M. Yaghi, Nature 427 (2004) 523–527.
[41] H. Li, M. Eddaoudi, T.L. Groy, O.M. Yaghi, J. Am. Chem. Soc. 120 (1998) 8571–8572.

[42] B. Chen, M. Eddaoudi, S.T. Hyde, M. O'Keeffe, O.M. Yaghi, Science 291 (2001) 1021–1023.
[43] B. Chen, M. Eddaoudi, T.M. Reineke, J.W. Kampf, M. O'Keeffe, O.M. Yaghi, J. Am. Chem. Soc. 122 (2000) 11559–11560.
[44] T.M. Reineke, M. Eddaoudi, M. O'Keeffe, O.M. Yaghi, Angew. Chem. Int. Ed. 38 (1999) 2590–2594.
[45] T.M. Reineke, M. Eddaoudi, M. Fehr, D. Kelley, O.M. Yaghi, J. Am. Chem. Soc. 121 (1999) 1651–1657.
[46] M. Eddaoudi, J. Kim, N. Rosi, D. Vodak, J. Wachter, M. O'Keeffe, O.M. Yaghi, Science 295 (2002) 469–472.
[47] H.K. Chae, M. Eddaoudi, J. Kim, S.I. Hauck, J.F. Hartwig, M. O'Keeffe, O.M. Yaghi, J. Am. Chem. Soc. 123 (2001) 11482–11483.
[48] K. Seki, W. Mori, J. Phys. Chem. B 106 (2002) 1380–1385.
[49] K. Barthelet, J. Marrot, D. Riou, G. Férey, Angew. Chem. Int. Ed. 41 (2002) 281–284.
[50] C. Serre, F. Millange, C. Thouvenot, M. Noguès, G. Marsolier, D. Louër, G. Férey, J. Am. Chem. Soc. 124 (2002) 13519–13526.
[51] M. Kondo, T. Yoshitomi, K. Seki, H. Matsuzaka, S. Kitagawa, Angew. Chem. Int. Ed. 36 (1997) 1725–1727.
[52] R. Nukada, W. Mori, S. Takamizawa, M. Mikuriya, M. Handa, H. Naono, Chem. Lett. 5 (1999) 367–368.
[53] M. Eddaoudi, H.L. Li, O.M. Yaghi, J. Am. Chem. Soc. 122 (2000) 1391–1397.
[54] A.J. Fletcher, E.J. Cussen, T.J. Prior, M.J. Rosseinsky, C.J. Kepert, K.M. Thomas, J. Am. Chem. Soc. 123 (2001) 10001–10011.
[55] L.C. Tabares, J.A.R. Navarro, J.M. Salas, J. Am. Chem. Soc. 123 (2001) 383–387.
[56] K. Seki, Chem. Commun. 16 (2001) 1496–1497.
[57] K. Seki, Langmuir 18 (2002) 2441–2443.
[58] D. Li, K. Kaneko, J. Phys. Chem. B 104 (2000) 8940–8945.
[59] B. Rather, M.J. Zaworotko, Chem. Commun. 7 (2003) 830–831.
[60] IUPAC Manual of Symbols and Terminology, Pure Appl. Chem. 31 (1972) 578.
[61] S. Brunauer, L.S. Deming, W.E. Deming, E. Teller, J. Am. Chem. Soc. 62 (1940) 1723–1732.
[62] S.J. Gregg, K.S.W. Sing, Adsorption, Surface Area and Porosity. 2nd ed., Academic Press, London, 1982.
[63] A.K. Cheetham, G. Férey, T. Loiseau, Angew. Chem. Int. Ed. 38 (1999) 3268–3292.
[64] C. Martin, N. Tosi-Pellenq, J. Patarin, J.P. Coulomb, Langmuir 14 (1998) 1774–1778.
[65] L. Mentasty, A.M. Woestyn, G. Zgrablich, Adsorpt. Sci. Technol. 11 (1994) 123–133.
[66] G.A. Ozin, A. Kuperman, A. Stein, Angew. Chem. 101 (1989) 373–390.
[67] B. Smit, T.L.M. Maesen, Nature 374 (1995) 42–44.
[68] K. Kaneko, K. Shimizu, T. Suzuki, J. Chem. Phys. 97 (1992) 8705–8711.
[69] K. Kaneko, K. Murata, Adsorption 3 (1997) 197–208.
[70] K.R. Matranga, A.L. Myers, E.D. Glandt, Chem. Eng. Sci. 47 (1992) 1569–1579.
[71] P.N. Aukett, N. Quirke, S. Riddiford, S.R. Tennison, Carbon 30 (1992) 913–924.
[72] R.K. Agarwal, J.A. Schwarz, J. Colloid Interface Sci. 130 (1989) 137–145.
[73] A. Corma, Chem. Rev. 97 (1997) 2373–2419.
[74] A.P. Malanoski, F. van Swol, Phys. Rev. E 66 (2002) 041602.
[75] F. Wendland, C. Naether, W. Bensch, Z. Naturforsch B59 (2004) 629–634.
[76] F.A.A. Paz, J. Klinowski, Inorg. Chem. 43 (2004) 3882–3893.
[77] G.J. Reiss, J.S. Engel, Z. Naturforsch B59 (2004) 1114–1117.
[78] R. Cao, Q. Shi, D. Sun, M. Hong, W. Bi, Y. Zhao, Inorg. Chem. 41 (2002) 6161–6168.
[79] Q.-Z. Wu, Y. Shen, Z.-F. Sun, Y.-G. Li, Wuji Cailiao Xuebao 19 (2004) 939–942.
[80] A.J. Fletcher, E.J. Cussen, D. Bradshaw, M.J. Rosseinsky, K.M. Thomas, J. Am. Chem. Soc. 126 (2004) 9750–9759.
[81] L. Gurvitsch, J. Phys. Chem. Soc. Russ. 47 (1915) 805.
[82] D. Dollimore, T. Shingles, J. Appl. Chem. 19 (1969) 218.
[83] J. Plévert, T.M. Gentz, A. Laine, H. Li, V.G. Young, O.M. Yaghi, M. O'Keeffe, J. Am. Chem. Soc. 123 (2001) 12706–12707.
[84] N. Khosrovani, A.W. Sleight, J. Solid State Chem. 121 (1996) 2–11.
[85] T. Takaishi, K. Tsutsumi, K. Chubachi, A. Matsumoto, J. Chem. Soc. Faraday Trans. 94 (1998) 601–608.
[86] T.G. Amos, A.W. Sleight, J. Solid State Chem. 160 (2001) 230–238.
[87] R.L. Withers, Y. Tabira, J.S.O. Evans, I.J. King, A.W. Sleight, J. Solid State Chem. 157 (2001) 186–192.
[88] D.C.S. Souza, V. Pralong, A.J. Jacobson, L.F. Nazar, Science 296 (2002) 2012–2015.
[89] S.-I. Noro, R. Kitaura, M. Kondo, S. Kitagawa, T. Ishii, H. Matsuzaka, M. Yamashita, J. Am. Chem. Soc. 124 (2002) 2568–2583.
[90] G.B. Gardner, D. Venkataraman, J.S. Moore, S. Lee, Nature 374 (1995) 792–795.
[91] K. Uemura, S. Kitagawa, M. Kondo, K. Fukui, R. Kitaura, H.-C. Chang, T. Mizutani, Chem. Eur. J. 8 (2002) 3586–3600.
[92] N. Rosi, M. Eddaoudi, J. Kim, M. O'Keeffe, O.M. Yaghi, Angew. Chem. Int. Ed. 41 (2002) 284–287.
[93] K. Biradha, M. Fujita, Angew. Chem. Int. Ed. 41 (2002) 3392–3395.
[94] R. Kitaura, K. Fujimoto, S.-I. Noro, M. Kondo, S. Kitagawa, Angew. Chem. Int. Ed. 41 (2002) 133–135.
[95] M.E. Kosal, J.-H. Chou, S.R. Wilson, K.S. Suslick, Nat. Mater. 1 (2002) 118–121.
[96] J.-H. Liao, S.-H. Cheng, C.-T. Su, Inorg. Chem. Commun. 5 (2002) 761–764.
[97] E.J. Cussen, J.B. Claridge, M.J. Rosseinsky, C.J. Kepert, J. Am. Chem. Soc. 124 (2002) 9574–9581.
[98] K. Biradha, Y. Hongo, M. Fujita, Angew. Chem. Int. Ed. 41 (2002) 3395–3398.
[99] C.J. Kepert, T.J. Prior, M.J. Rosseinsky, J. Am. Chem. Soc. 122 (2000) 5158–5168.
[100] D.V. Soldatov, J.A. Ripmeester, S.I. Shergina, I.E. Sokolov, A.S. Zanina, S.A. Gromilov, Y.A. Dyadin, J. Am. Chem. Soc. 121 (1999) 4179–4188.
[101] D.V. Soldatov, J.A. Ripmeester, Chem. Mater. 12 (2000) 1827–1839.
[102] D. Li, K. Kaneko, Chem. Phys. Lett. 335 (2001) 50–56.
[103] L. Carlucci, G. Ciani, M. Moret, D.M. Proserpio, S. Rizzato, Angew. Chem. Int. Ed. 39 (2000) 1506–1510.
[104] J.Y. Lu, A.M. Babb, Chem. Commun. 13 (2002) 1340–1341.
[105] H. Li, C.E. Davis, T.L. Groy, D.G. Kelley, O.M. Yaghi, J. Am. Chem. Soc. 120 (1998) 2186–2187.
[106] S.K. Makinen, N.J. Melcer, M. Parvez, G.K.H. Shimizu, Chem. Eur. J. 7 (2001) 5176–5182.
[107] G.B. Gardner, Y.-H. Kiang, S. Lee, A. Asgaonkar, D. Venkataraman, J. Am. Chem. Soc. 118 (1996) 6946–6953.
[108] S. Naito, T. Tanibe, E. Saito, T. Miyao, W. Mori, Chem. Lett. 11 (2001) 1178–1179.
[109] C.J. Kepert, D. Hesek, P.D. Beer, M.J. Rosseinsky, Angew. Chem. Int. Ed. 37 (1998) 3158–3160.
[110] K. Nagayoshi, M.K. Kabir, H. Tobita, K. Honda, M. Kawahara, M. Katada, K. Adachi, H. Nishikawa, I. Ikemoto, H. Kumagai, Y. Hosokoshi, K. Inoue, S. Kitagawa, S. Kawata, J. Am. Chem. Soc. 125 (2003) 221–232.
[111] H.J. Choi, T.S. Lee, M.P. Suh, Angew. Chem. Int. Ed. 38 (1999) 1405–1408.

[112] D.V. Soldatov, A.T. Henegouwen, G.D. Enright, C.I. Ratcliffe, J.A. Ripmeester, Inorg. Chem. 40 (2001) 1626–1636.
[113] S. Takamizawa, T. Saito, T. Akatsuka, E. Nakata, Inorg. Chem. 44 (2005) 1421–1424.
[114] R. Kitaura, K. Seki, G. Akiyama, S. Kitagawa, Angew. Chem. Int. Ed. 42 (2003) 428–431.
[115] K. Seki, Phys. Chem. Chem. Phys. 4 (2002) 1968–1971.
[116] D. Maspoch, D. Ruiz-Molina, K. Wurst, N. Domingo, M. Cavallini, F. Biscarini, J. Tejada, C. Rovira, J. Veciana, Nat. Mater. 2 (2001) 190–195.
[117] G.J. Halder, C.J. Kepert, J. Am. Chem. Soc. 127 (2005) 7891–7900.
[118] S. Uchida, R. Kawamoto, T. Akatsuka, S. Hikichi, N. Mizuno, Chem. Mater. 17 (2005) 1367–1375.
[119] M.P. Suh, J.W. Ko, H.J. Choi, J. Am. Chem. Soc. 124 (2002) 10976–10977.
[120] M.J. Bojan, W.A. Steele, Carbon 36 (1998) 1417–1423.
[121] X. Yang, J. Ding, J. Chem. Phys. 121 (2004) 7449–7456.
[122] S. Kitagawa, M. Kondo, Bull. Chem. Soc. Jpn. 71 (1998) 1739–1753.
[123] S. Takamizawa, E.-I. Nakata, H. Yokoyama, K. Mochizuki, W. Mori, Angew. Chem. Int. Ed. 42 (2003) 4331–4334.
[124] O.M. Yaghi, H. Li, J. Am. Chem. Soc. 118 (1996) 295–296.
[125] K.S. Min, M.P. Suh, J. Am. Chem. Soc. 122 (2000) 6834–6840.
[126] O.-S. Jung, Y.J. Kim, Y.-A. Lee, J.K. Park, H.K. Chae, J. Am. Chem. Soc. 122 (2000) 9921–9925.
[127] O.-S. Jung, Y.J. Kim, Y.-A. Lee, H.K. Chae, H.G. Jang, J. Hong, Inorg. Chem. 40 (2001) 2105–2110.
[128] B.F. Abrahams, M.J. Hardie, B.F. Hoskins, R. Robson, G.A. Williams, J. Am. Chem. Soc. 114 (1992) 10641–10643.
[129] S. Muthu, J.H.K. Yip, J.J. Vittal, J. Chem. Soc. Dalton 24 (2002) 4561–4568.
[130] A.N. Khlobystov, N.R. Champness, C.J. Roberts, S.J.B. Tendler, C. Thompson, M. Schroder, Cryst. Eng. Commun. (2002) 426–431.
[131] T.J. Wadas, Q.-M. Wang, Y.-J. Kim, C. Flaschenreim, T.N. Blanton, R. Eisenberg, J. Am. Chem. Soc. 126 (2004) 16841–16849.
[132] R. Matsuda, R. Kitaura, S. Kitagawa, Y. Kubota, T.C. Kobayashi, S. Horike, M. Takata, J. Am. Chem. Soc. 126 (2004) 14063–14070.
[133] M. Alvaro, B. Ferrer, H. Garcia, F. Rey, Chem. Commun. 18 (2002) 2012–2013.
[134] N.K. Mal, M. Fujiwara, Y. Tanaka, Nature 421 (2003) 350–353.
[135] D.V. Soldatov, I.L. Moudrakovski, C.I. Ratcliffe, R. Dutrisac, J.A. Ripmeester, Chem. Mater. 15 (2003) 4810–4818.
[136] K. Uemura, S. Kitagawa, K. Fukui, K. Saito, J. Am. Chem. Soc. 126 (2004) 3817–3828.
[137] L. Pan, K.M. Adams, H.E. Hernandez, X. Wang, C. Zheng, Y. Hattori, K. Kaneko, J. Am. Chem. Soc. 125 (2003) 3062–3067.
[138] H.P. Boehm, M. Voll, Carbon 8 (1970) 227–240.
[139] M. Voll, H.P. Boehm, Carbon 9 (1971) 481–488.
[140] M. Kondo, M. Shimamura, S.-I. Noro, S. Minakoshi, A. Asami, K. Seki, S. Kitagawa, Chem. Mater. 12 (2000) 1288–1299.
[141] K. Seki, S. Takamizawa, W. Mori, Chem. Lett. 4 (2001) 332–333.
[142] K. Seki, S. Takamizawa, W. Mori, Chem. Lett. 2 (2001) 122–123.
[143] W. Mori, H. Hoshino, Y. Nishimoto, S. Takamizawa, Chem. Lett. 4 (1999) 331–332.
[144] United States Department of Energy, Available online at http://www.eere.energy.gov/hydrogenandfuelcells/pdfs/h2_storage_think_tank.pdf.
[145] L. Schlapbach, A. Züttel, Nature 414 (2001) 353–358.
[146] M.G. Nijkamp, J.E.M.J. Raaymakers, A.J. van Dillen, K.P. de Jong, Appl. Phys. A: Mater. 72 (2001) 619–623.
[147] X.B. Zhao, B. Xiao, A.J. Fletcher, K.M. Thomas, J. Phys. Chem. B 109 (2005) 8880–8888.
[148] J. Pang, J.E. Hampsey, Z. Wu, Q. Hu, Y. Lu, Appl. Phys. Lett. 85 (2004) 4887–4889.
[149] A.C. Dillon, K.M. Jones, T.A. Bekkedahl, C.H. Kiang, D.S. Bethune, M.J. Heben, Nature 386 (1997) 377–379.
[150] A. Chambers, C. Park, R.T.K. Baker, N.M. Rodriguez, J. Phys. Chem. B 102 (1998) 4253–4256.
[151] C. Park, P.E. Anderson, A. Chambers, C.D. Tan, R. Hidalgo, N.M. Rodriguez, J. Phys. Chem. B 103 (1999) 10572–10581.
[152] C.C. Ahn, Y. Ye, B.V. Ratnakumar, C.J. Witham, R.C.J. Bowman, B. Fultz, Appl. Phys. Lett. 73 (1998) 3378–3380.
[153] F.E. Pinkerton, B.G. Wicke, C.H. Olk, G.G. Tibbets, G.P. Meisner, M.S. Meyer, J.F. Herbst, J. Phys. Chem. B 104 (2000) 9460–9467.
[154] H.G. Schimmel, G.J. Kearly, M.G. Nijkamp, C.T. Visser, K.P. de Jong, F.M. Mulder, Chem. Eur. J. 9 (2003) 4764–4770.
[155] G. Gundiah, A. Govindaraj, N. Rajalakshmi, K.S. Dhathathreyan, C.N.R. Rao, J. Mater. Chem. 13 (2003) 209–213.
[156] M. Becher, M. Haluska, M. Hirscher, A. Quintel, V. Skakalova, U. Dettlaff-Weglikovska, X. Chen, M. Hulman, Y. Choi, S. Roth, V. Meregalli, M. Parrinello, R. Strobel, L. Jorissen, M.M. Kappes, J. Fink, A. Züttel, I. Stepanek, P. Bernier, Comptes Rendes Phys. 4 (2003) 1055–1062.
[157] P. Benard, R. Chahine, Langmuir 17 (2001) 1950–1955.
[158] G.G. Tibbetts, G.P. Meisner, C.H. Olk, Carbon 39 (2001) 2291–2301.
[159] M. Rzepka, P. Lamp, M.A. de la Casa-Lillo, J. Phys. Chem. B 102 (1998) 10894–10898.
[160] M. Dresselhaus, K.A. Williams, P.C. Eklund, MRS Bull. 24 (1999) 45–50.
[161] A. Züttel, P. Sudan, P. Mauron, T. Kiyobayashi, C. Emmenegger, L. Schlapbach, Int. J. Hydrogen Energy 27 (2002) 203–212.
[162] G. Sandrock, J. Alloy Compd. 293–295 (1999) 877–888.
[163] R.C.J. Bowman, B. Fultz, MRS Bull. 27 (2002) 688–693.
[164] J. Weitkamp, M. Fritz, S. Ernst, Int. J. Hydrogen Energy 20 (1995) 967–970.
[165] Y. Ye, C.C. Ahn, C. Witham, B. Fultz, J. Liu, A.G. Rinzler, D. Colbert, K.A. Smith, R.E. Smalley, Appl. Phys. Lett. 74 (1999) 2307–2309.
[166] C. Liu, Y.Y. Fan, M. Liu, H.T. Cong, H.M. Cheng, M.S. Dresselhaus, Science 285 (1999) 1127–1129.
[167] C.M. Brown, T. Yildirim, D.A. Neumann, M.J. Heben, T. Gennett, A.C. Dillon, J.L. Alleman, J.E. Fischer, Chem. Phys. Lett. 329 (2000) 311–316.
[168] A. Kuznetsova, D.B. Mawhinney, V. Naumenko, J.T.J. Yates, J. Liu, R.E. Smalley, Chem. Phys. Lett. 321 (2000) 292–296.
[169] R.T. Yang, Carbon 38 (2000) 623–626.
[170] H.W. Zhu, A. Chen, Z.Q. Mao, C.L. Xu, X. Xiao, B.Q. Wei, L. Liang, D.H. Wu, J. Mater. Sci. Lett. 19 (2000) 1237–1239.
[171] V. Meregalli, M. Parrinello, Appl. Phys. A: Mater. 72 (2001) 143–146.
[172] A.C. Dillon, M.J. Heben, Appl. Phys. A: Mater 72 (2001) 133–142.
[173] B. Bogdanovic, M. Schwickardi, J. Alloy Compd. 253–254 (1997) 1–9.
[174] F. Schuth, B. Bogdanovic, M. Felderhoff, Chem. Commun. 20 (2004) 2249–2258.
[175] J.L.C. Rowsell, A.R. Millward, K.S. Park, O.M. Yaghi, J. Am. Chem. Soc. 126 (2004) 5666–5667.
[176] L. Pan, M.B. Sander, X. Huang, J. Li, M. Smith, E. Bittner, B. Bockrath, J.K. Johnson, J. Am. Chem. Soc. 126 (2004) 1308–1309.
[177] B. Panella, M. Hirshcer, Adv. Mater. 17 (2005) 538–541.

[178] P.M. Forster, J. Eckert, J.-S. Chang, S.-E. Park, G. Férey, A.K. Cheetham, J. Am. Chem. Soc. 125 (2003) 1309–1312.
[179] G. Férey, M. Latroche, C. Sérre, F. Millange, T. Loiseau, A. Percheron-Guegan, Chem. Commun. 24 (2003) 2976–2977.
[180] T. Loiseau, C. Serre, C. Huguenard, G. Fink, G. Taulelle, M. Henry, T. Bataille, G. Férey, Chem. Eur. J. 10 (2004) 1373–1382.
[181] F. Millange, C. Serre, G. Férey, Chem. Commun. 8 (2002) 822–823.
[182] D.N. Dybtsev, H. Chun, S.H. Yoon, D. Kim, K. Kim, J. Am. Chem. Soc. 126 (2004) 32–33.
[183] S.D.M. Brown, G. Dresselhaus, M.S. Dresselhaus, Mater. Res. Soc. Symp. Proc. 497 (1998) 157–163.
[184] O. Gulseren, T. Yildirim, S. Ciraci, Phys. Rev. Lett. 87 (2001) 116802/1–116802/4.
[185] K. Kadano, H. Kajiura, M. Shiraishi, Appl. Phys. Lett. 83 (2003) 3392–3394.
[186] K. Shen, T. Pietrass, J. Phys. Chem. B 108 (2004) 9937–9942.
[187] J.B. Parra, C.O. Ania, A. Arenillas, F. Rubiera, J.M. Palacios, J.J. Pis, J. Alloy Compd. 379 (2004) 280–289.